EFFECT OF THERMAL CYCLING ON SLURRY EROSIVE BEHAVIOUR OF MEDIUM CARBON LOW ALLOY STEEL

A DISSERTATION

Submitted in partial fulfillment of the

requirements for the award of the degree

of

MASTER OF TECHNOLOGY

In

DEPARTMENT OF METALLURGICAL AND MATERIALS ENGINEERING

(With Specialization in Industrial Metallurgy)

By

RAKESH AHLAWAT

DEPARTMENT OF METALLURGICAL AND MATERIALS ENGINEERING

INDIAN INSTITUTE OF TECHNOLOGY ROORKEE

ROORKEE – 247667 (INDIA)

MAY, 2016

CANDIDATE'S DECLARATION

I hereby declare that the work presented in this dissertation entitled "**Effect of thermal cycling on slurry erosive behaviour of medium carbon low alloy steel"** in partial fulfillment of the requirement for the award of the degree of **Masters of Technology** in **Metallurgical and Materials Engineering** with specialization in **Industrial Metallurgy,** submitted in the **Department of Metallurgical and Materials Engineering, Indian Institute of Technology, Roorkee** is an authentic record of my own work carried out during the period from July 2015 to May 2016 under the supervision of **Dr. Sumeer K. Nath,** Professor, Department of Metallurgical and Materials Engineering, Indian Institute of Technology, Roorkee.

The matter presented in this dissertation has not been submitted by me for the award of any other degree.

Dated: **RAKESH AHLAWAT**

Place: Roorkee **Enrollment no. - 14544016**

CERTIFICATE

This is to certify that above statement made by the candidate is correct to the best of my knowledge and belief.

Dr. Sumeer K. Nath

Professor

Department of Metallurgical and Materials Engineering

Indian Institute of Technology, Roorkee

Roorkee-247667 (INDIA)

ACKNOWLEDGEMENT

I would like to thank the almighty God for giving me strength to accomplish my work with honor. I am highly indebted to **Dr. Sumeer K. Nath,** Professor, Metallurgical and Materials Engineering, Indian Institute of Technology Roorkee, for encouraging me to undertake this dissertation as well as providing me all the necessary guidance and inspirational support throughout this dissertation work. He has displayed unique tolerance and understanding at every step of progress. It is my proud privilege to have carried out this dissertation work under his able guidance.

I wish to express my sincere thanks to **Dr. Anjan Sil,** Professor and Head of the Department, Metallurgical and Materials Engineering Department, Indian Institute of Technology Roorkee, for his help to carry out this dissertation.

I also like to express my gratitude to Mr. Guru Prakash, Mr. Sanjeev Kumar and Mr. Sumit Kumar, Research Scholar for their innumerable discussion, his generosity and willingness to share his knowledge. I sincerely appreciate his valuable persistent encouragement in making this work.

Sincere thanks to technical staff of MMED who worked with me as friends, Mr. Rajendra Sharma and Mr. Naresh Sharma.

I would like to acknowledge all my friends specially Mr. Niranjan, Mr. Kapil and Mr. Vipin Kumar for their valuable information share, and developing love and confidence in me throughout the work. Last but not the least I would like to thanks my parents who have been a constant source of my inspiration to me.

(RAKESH AHLAWAT)

Table of Contents

List of Figures

List of Tables

Abstract

Slurry erosive wear is defined as the phenomenon of material removal from the surface by the impact of solid particle flowing in fluid at certain velocity and angle. Slurry erosion is important in various engineering applications such as oil and gas industry, pipeline systems, pumps, hydraulic machinery, etc. So, improving the performance of medium carbon low alloy steel which is mostly used in above said engineering applications leads to economic development of any country. Steel microstructure, which directly influences its strength, hardness and toughness, plays an important role in determining the wear rate.

The objective of this project is to study the effect of thermal cycling on slurry erosion behaviour of 0.43 C wt. % low alloy steel. Thermal cycling is done on spheroidized, annealed and normalized medium carbon low alloy steel and cycling effect on different initial morphology is studied. Thermal cycling consists of alternate heating and cooling at 50ºC above and below A3 temperature (852ºC) with holding time of 3 min. at both temperatures. Heating and cooling rate for thermal cycling is 5ºC/s. Thermal cycling results in variety of microstructures and mechanical properties. The slurry erosion tests were performed on slurry erosion pot test apparatus using silica sand particles (size – 212 to 300µm) as erodent. Weight loss was calculated after every 3 hr. time interval and total test time was 24 hr. The experimental findings reveal that thermal cycling improves slurry erosion resistance. It was found that cumulative weight loss shows direct relationship with hardness with respect to similar morphology materials. Minimum weight loss is observed in case of two time thermal cycled annealed material (57% decrement w.r.t. as-received spheroidized material). The microstructures and worn out surfaces were analyzed by optical microscopy and field emission scanning electron microscopy.

Chapter 1
Introduction

1.1 Steel

Steel is an alloy of iron and carbon (primarily), where carbon goes on interstitial sites. It is one of the most important engineering material in the world. It is world's most produced material due to its efficient and less costly production methods. It is used in almost all engineering or non-engineering sector. That's why a famous phrase is generally said that – "Steel can only be replaced by steel". So there is a lot of research left in the field of improvement of properties of steel.

Steel is mainly divided into two categories –

1. Plain Carbon Steels – Carbon is the only alloying element and based on carbon weight %, these steels are further divided into low (up to 0.3%), medium (0.3% to 0.6%) and high (0.6% to 2.1%) carbon steels. Strength and hardness increases with increase in carbon percentage but ductility and weld ability decreases.

2. Alloy steels – Alloying elements are added to increase the selective property of steel. Different alloying elements improve different mechanical properties. For example – C increases strength, hardness and wear; Cr increases wear and corrosion resistance; Co prevents grain growth; Mn increases hardenability; Mo increases wear resistance; Pb and S increase machinability and Cu increases corrosion resistance etc.

Medium carbon low alloy steel has high strength to weight ratio, superior toughness and good machinability. This steel has wide range of applications such as – slurry pipes, turbine parts, power plant industry, rock-processing machinery, aerospace and automobile industry etc.

1.2 Heat Treatment

Heat treatment is a controlled heating and cooling process used to change the morphology and mechanical properties of most of the metals. Steel properties are widely changed with different heat treatment processes.

Some of the common heat treatment processes are –

1. Annealing – Annealing is the heat treatment process used for stress relieving, refining grain structure and restoring ductility. In this process, first the steel sample is heated to austenite region (50ºC above A_3/A_{cm} line) and held there for sufficient time till complete homogenization took place and after that equilibrium or furnace cooling is done. After annealing, the steel becomes very soft and ductile due to coarse grain ferrite/pearlite or cementite/pearlite microstructure.

2. Normalizing – Normalizing is same process as annealing except cooling process. In case of normalizing, air cooling is done. So this process is less costly than annealing and also time saving process. After normalizing, the steel becomes strong, hard and less ductile as compared to annealing due to fine grain ferrite/pearlite or cementite/pearlite microstructure.

3. Spheroidization – Spheroidization process is generally used to increase machinability of medium/high carbon steels. This process is done in three ways – heating the steel just below A_1 line for several hours and then slow cooling, cyclic heating above and below A_1 line for multiple times and then slow cooling and lastly, in case of alloy steels, heating to inter-critical region and holding their for several hours followed by slow cooling. These all three processes lead to a morphology having cementite spheroids in ferrite matrix.

4. Hardening – Quenching is the hardening process. It is the non-diffusional transformation process in which austenite is transformed to martensite upon very fast cooling or water cooling. Martensite is very hard phase and also very brittle. So for practical applications it is of no use due to its brittleness. Tempering is done to provide some ductility to the quenched product and to make it useful for practical applications. In this process, the quenched product is heated to a temperature below A_1 line. During heating, carbon atoms diffuses from martensite and forms carbide precipitates which provides ductility.

The heating range of all the heat treatment processes is shown in Fig. 1.1.

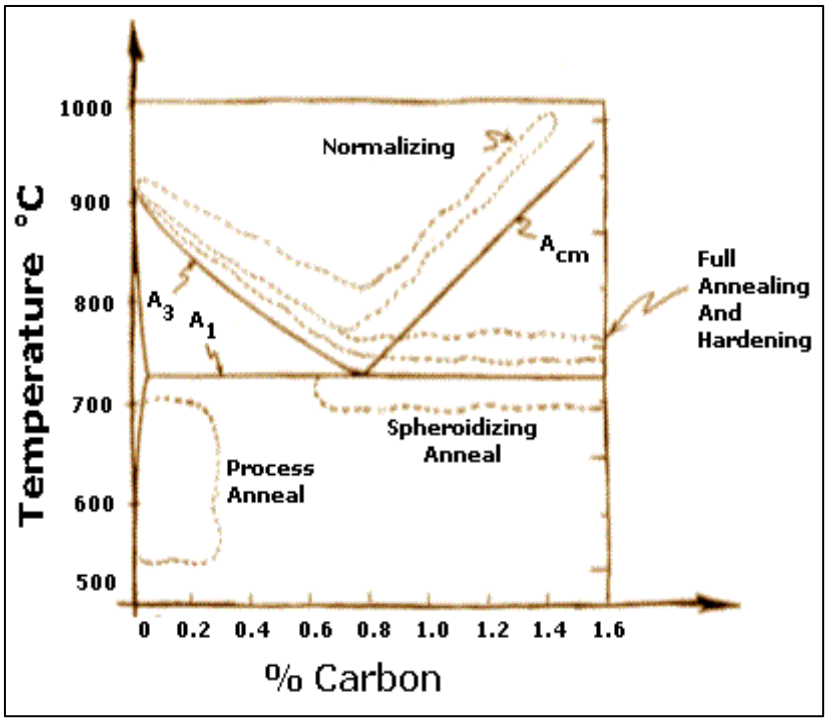

Fig. 1.1 Heat treatment processes

1.3 Thermal cycling

Thermal cycling heat treatment is not new process to us. It is similar to cyclic heating done in spheroidization process along A_1 temperature so that ductility of material also got improved with addition to its strength and hardness [1].

Two main advantages of thermal cycling are –

1. Faster kinetics as compared to conventional spheroidization process [2]. Generally spheroidization is done to increase ductility of high carbon steel and conventional spheroidization process took 70-80 hours for complete spheroidization in the material while using thermal cycling process, complete spheroidization occurs in about only 1 hour.

2. Good combination of strength, hardness and toughness [1][2][3]

3. Oxidation and decarburization of steel is minimum and protective atmospheres are not required [4]

A schematic view of thermal cycling is shown in Fig. 1.2.

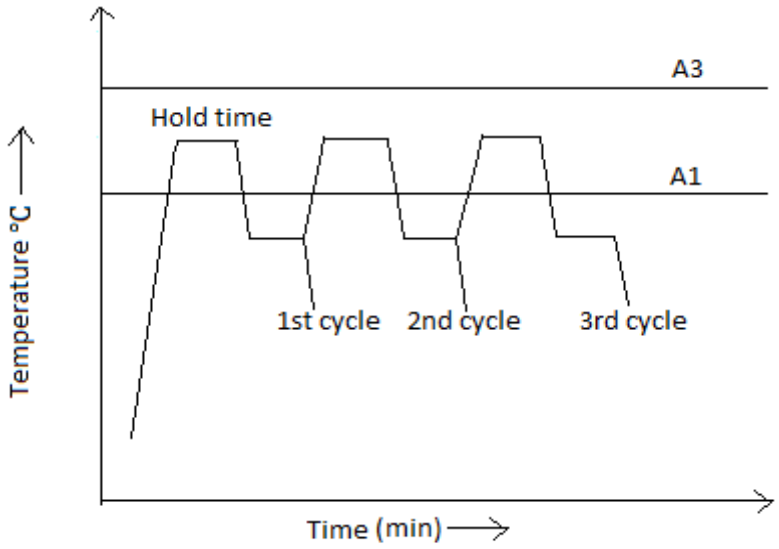

Fig. 1.2 Schematic representation of thermal cycling

Holding time plays an important role in fineness of grain size. Due to short hold time, cementite does not dissolve completely in austenite because cementite dissolution is diffusional transformation. So, incomplete dissolution of cementite impedes the grain growth of austenite due to which fine grain microstructure obtained. Finer grains results in increased strength and hardness according to Hall-Patch equation [5]. Four to five cycles are sufficient for improvement of mechanical properties as more cycles results in micro-crack generation, less hardenability due to refinement of previous austenite grain, not economical and negative effects due to micro-deformation processes [6].

1.4 Slurry Erosion

Slurry erosive wear is defined as the phenomenon of material removal from the surface by the impact of solid particle flowing in fluid at certain velocity and angle. Slurry erosion is important in various engineering applications such as oil and gas industry, pipeline systems, pumps, hydraulic machinery, etc. Estimated direct and consequential annual loss to industrial nations due to wear is approximately 1-2% of GDP. A study estimated that the cost of friction and wear in India is Rs.78.67 billion and 55-60 % of equipment damage is caused by poor lubrication and severe wear [7].

So, improving the performance of medium carbon low alloy steel which is mostly used in above engineering applications leads to economic development of any country. Slurry erosion depends on both slurry and specimen characteristics. Slurry characteristics include slurry concentration, pH of slurry, size, shape, hardness, velocity and impingement angle of erodent particles. Specimen characteristics include morphology and mechanical properties (strength, hardness, ductility etc.) [8].

General equation representing volume loss due to wear (V) is expressed as shown in eq. 1 [9] :

$$V = \frac{\frac{1}{2mv^2}}{H} f(\alpha) \qquad \ldots\ldots\ldots\ldots\ldots\ldots (1)$$

where m is mass of particle, v is velocity, H is hardness and α is impingement angle.

The lower angle of impingement (20-30º) yields higher wear volume loss in ductile materials and at higher impingement angle (80-90º) wear volume loss is higher in brittle materials. So ductility or brittleness both play different role in erosive wear volume loss.

Chapter 2

Literature Survey

2.1 Thermal cycling

2.1.1 Low carbon steel

Atanu Saha et al. [3] had investigated the thermal cycling effects on microstructure and mechanical properties of 0.16% carbon steel. Fig. 2.1 shows the diagram of applied cyclic heat treatment –

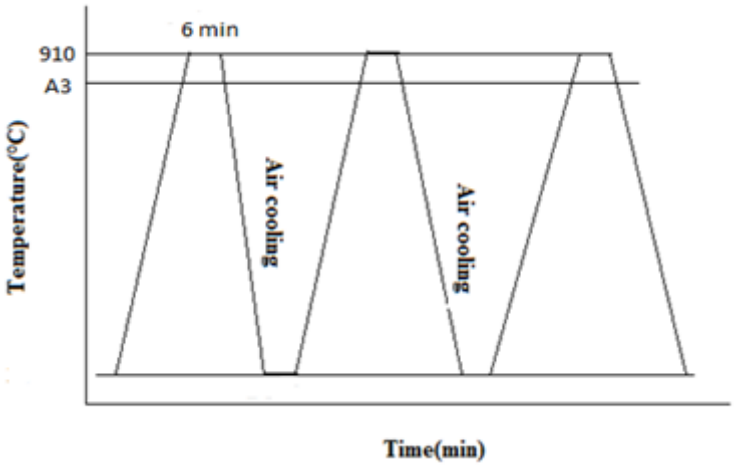

Fig. 2.1 Rapid cyclic heat treatment [3]

Due to short duration holding (6 min.) at 910ºC, undissolved cementite impedes the growth of nucleated austenite grains. The grain size of ferrite grains reduced to 7µm after 8 cycles from 47µm (annealed sample). Good combination of strength (338 MPa from 200 MPa), hardness (135 HV from 103 HV) and ductility (36% from 42%) obtained after 2nd cycle of heat treatment due to fine ferrite grain size, high dislocation density of ferrite grains, an adequate amount of fine lamellar pearlite and lower proportion of grain boundary cementite in the microstructure. After 2nd cycle, strength and hardness decreases whereas ductility increases. Cementite clusters acts as failure initiation sites and relatively lower strength is achieved after 2nd cycle of heat treatment. Cementite network is not continuous across ferrite grain boundary so overall fracture is not inter-granular, rather trans-granular dimple rupture through micro void coalescences therefore ductility not reduced after 2nd cycle.

J.Y.Koo and G.Thomas [10] had investigated the effect of thermal cycling and conventional cycling on mechanical properties of 1010 alloy steel. Fig. 2.2 shows schematic diagram of conventional and experimental thermal cycles –

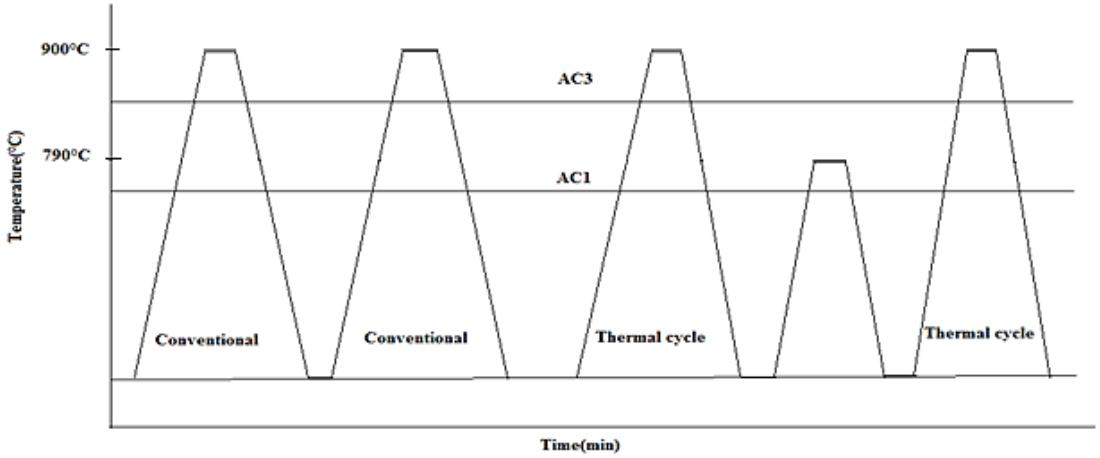

Fig. 2.2 Schematic sketch of conventional and experimental thermal cycles [10]

It was found that experimental thermal cycles provide fine grain micro constituents than conventional thermal cycles. It was investigated that second phase (proeutectoid ferrite) restricts the grain growth of austenite in inter-critical region. Experimental thermal cycling provides better combination of yield strength and uniform elongation than conventional thermal cycling i.e. 15-20 k.s.i. increase in yield strength at similar elongation or 2-3% increase in uniform elongation at similar yield strengths. Also it was investigated that grain refinement occurs only up to two cycles and after two cycles there is no additional improvement in tensile properties.

2.1.2 Medium carbon steel

Atanu Saha et al. [11] studied the effect of cyclic heat treatment on microstructure and mechanical properties of 0.6 wt. % carbon steel. Cyclic heat treatment consisted of alternating heating and cooling of annealed sample between 810ºC (50ºC above A_3) and room temperature with holding time of 6 min. at both temperatures. Incomplete dissolution of cementite due to short time holding at 810ºC restricts the grain growth of austenite grains. As a result of forced air cooling, fine ferrite grains obtained. Also due to non-equilibrium forced air cooling, ‘lamellar fault’ regions generated and these regions acts as potential sites for spheroidization. So as no. of thermal cycles increased, volume fraction of fine ferrite and spheroidized cementite increases. Best results are obtained after 5 cycles. On reaching 5^{th} cycle, yield strength increased to

486 MPa from 324 MPa, hardness increased to 230 HV from 202 HV and ductility remains nearly same i.e. 30%. Strength property increased as a result of finer micro-constituents and due to small size cementite spheroids dispersed in fine ferrite matrix, ductility do not reduces. After 5^{th} cycle, strength marginally decreases due to elimination of lamellar pearlite and increment in volume fraction of cementite spheroids. So thermal cycling resulted in excellent combination of strength, hardness and ductility.

Bozo Smoljan [6] had investigated the strengthening of AISI 4140 steel by cyclic heat treatment combined (diffusional transformation) with quenching (diffusion-less transformation). Complete heat treatment process consists of grain refinement by repeated α-ferrite ↔ γ-ferrite transformations and further quenching and tempering were done. Fig. 2.3 shows the diagram of applied combined cyclic heat treatment –

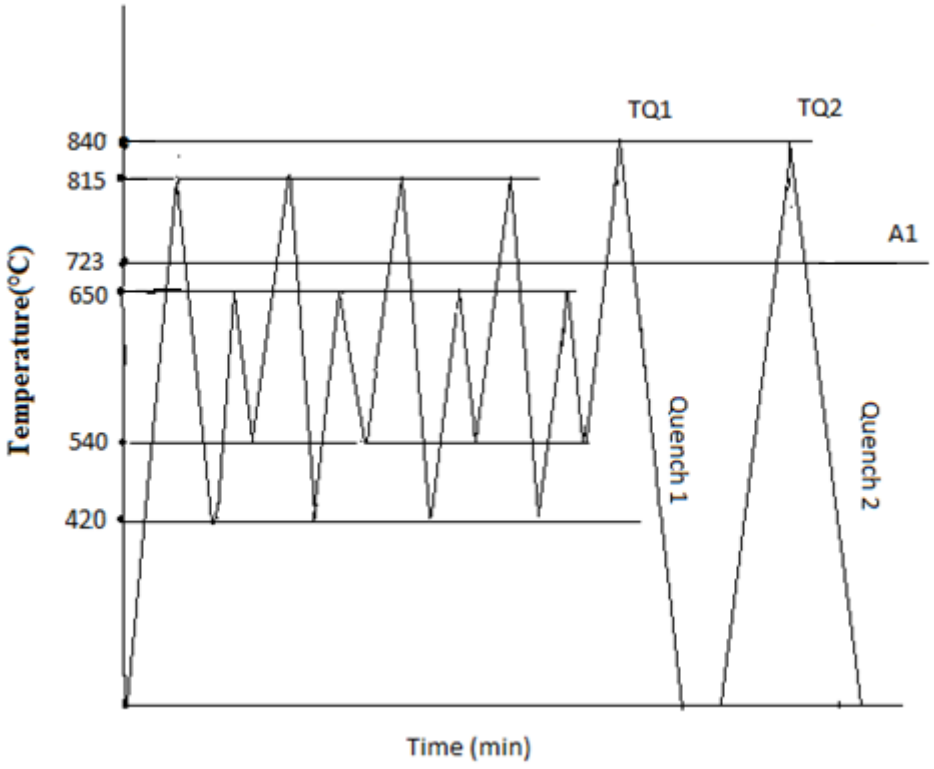

Fig. 2.3 Combined cyclic heat treatment containing both diffusion and diffusionless transformation [6]

It was observed that after combined cyclic heat treatment performance, material shows good results of strength and toughness as compared to results obtained after direct quenching and tempering process due to grain refinement.

Mahajan et al. [12] correlated the mechanical behaviour of commercial medium carbon steel (C-0.40, Mn-0.78, Cr-1.1, Mo-0.2) with microstructure and micro-fracture after rapid cyclic heating. Applied cyclic heat treatment consisted of alternate heating and cooling between austenitization and room temperature with a holding time of 6 min. at each temperature. Rapid re-austenitizing was carried out in vacuum with heating rates of 170ºC/sec, 245ºC/sec, 300ºC/sec and 440ºC/sec. It was found that grain size reduced from 25µm to 4µm after fourth cycle. It has been investigated that proof stress increment is due to refinement of grain size and fine precipitates of carbide in ferrite matrix.

Birger karlson [13] had studied that repetitive short time austenitization results in grain refinement. Fig. 2.4 shows the applied thermal cycling to improve mechanical properties –

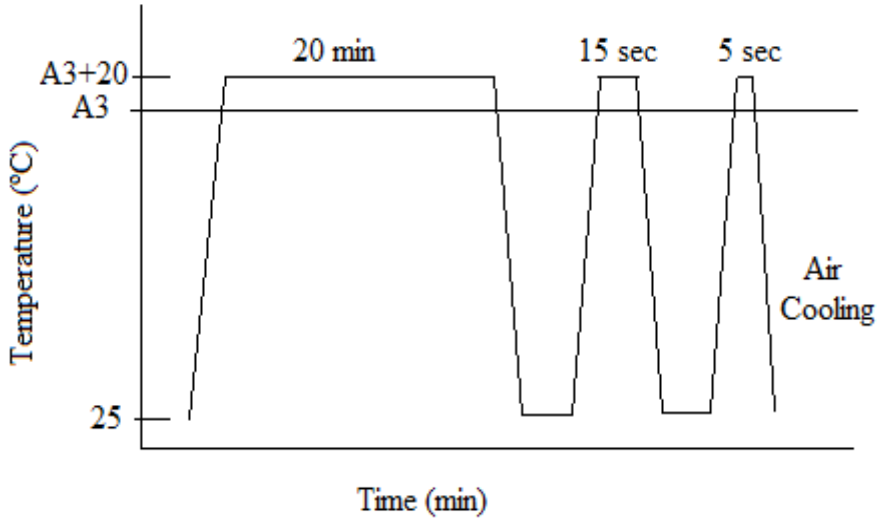

Fig. 2.4 Thermal cycling showing short time repetitive austenitization [13]

Different carbon content steels were investigated: 0.05, 0.18 and 0.38 wt. % C. It was found that thermal cycling results in reduction of grain size of up to 1:10 in ferritic-pearlitic condition. Grain refinement occurs due to rapid nucleation of ferritic grain during fast cooling. Grain refinement is more in case of high carbon steels and of material having initial grain size near to 100µm.

2.1.3 High carbon steel

Saha et al. [2] had investigated that cyclic heat treatment process on annealed 1.24 wt. % carbon steel results in high strength ductile hypereutectoid steel. Cyclic heat treatment consisted of alternating heating and cooling of annealed sample between

894ºC (50ºC above A_{cm}) and room temperature with holding time of 6 min. at both temperatures. Initially homogenized annealed specimen has poor ductility due to presence of brittle cementite network. On increasing no. of thermal cycles, non-lamellar pearlite region increases and ductility property increases due to elimination of brittle cementite network. During short holding time, cementite remains undissolved and then non-equilibrium forced air cooling results in lamellar fault generation. These lamellar faults accelerate the fragmentation of cementite particles and size of cementite particles reduces and more uniformly dispersed in ferrite matrix. So it was concluded that cyclic heat treatment results in finer micro-constituents and also accelerates spheroidization. Strength increases mainly due to reduction of grain size and increment in ductility was due to fine spheroidal cementite particles in ferrite matrix.

Z.Q. Lv et al. [1] had investigated that rapid thermal cycling about A_1 temperature results in spheroidization of high carbon steel. Fig. 2.5 shows the schematic diagram of applied thermal cycle in this work –

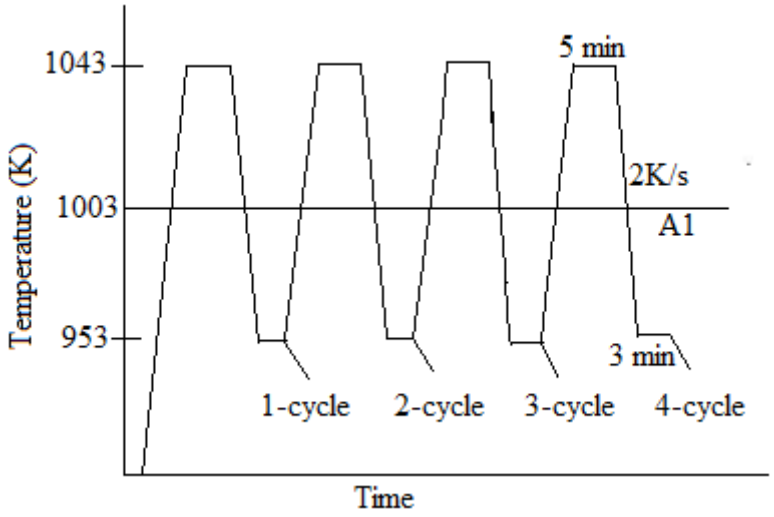

Fig. 2.5 Thermal cycling curve for spheroidization [1]

It was found that 100% spheroidization occurs after 5^{th} cycle. Elongation increases to 25.4% after 5^{th} cycle from 8% of base material without any considerable decrement in ultimate tensile strength.

2.2 Slurry erosion

Mechanism of slurry erosion: Due to impact of solid particles on the target material, indentation occurs and repeated impacting by solid particles gradually removes material from the surface of target material through repeated plastic deformation, cutting and ploughing actions [14]. In case of brittle materials, repeated impacting leads to crack generation and fracture happens.

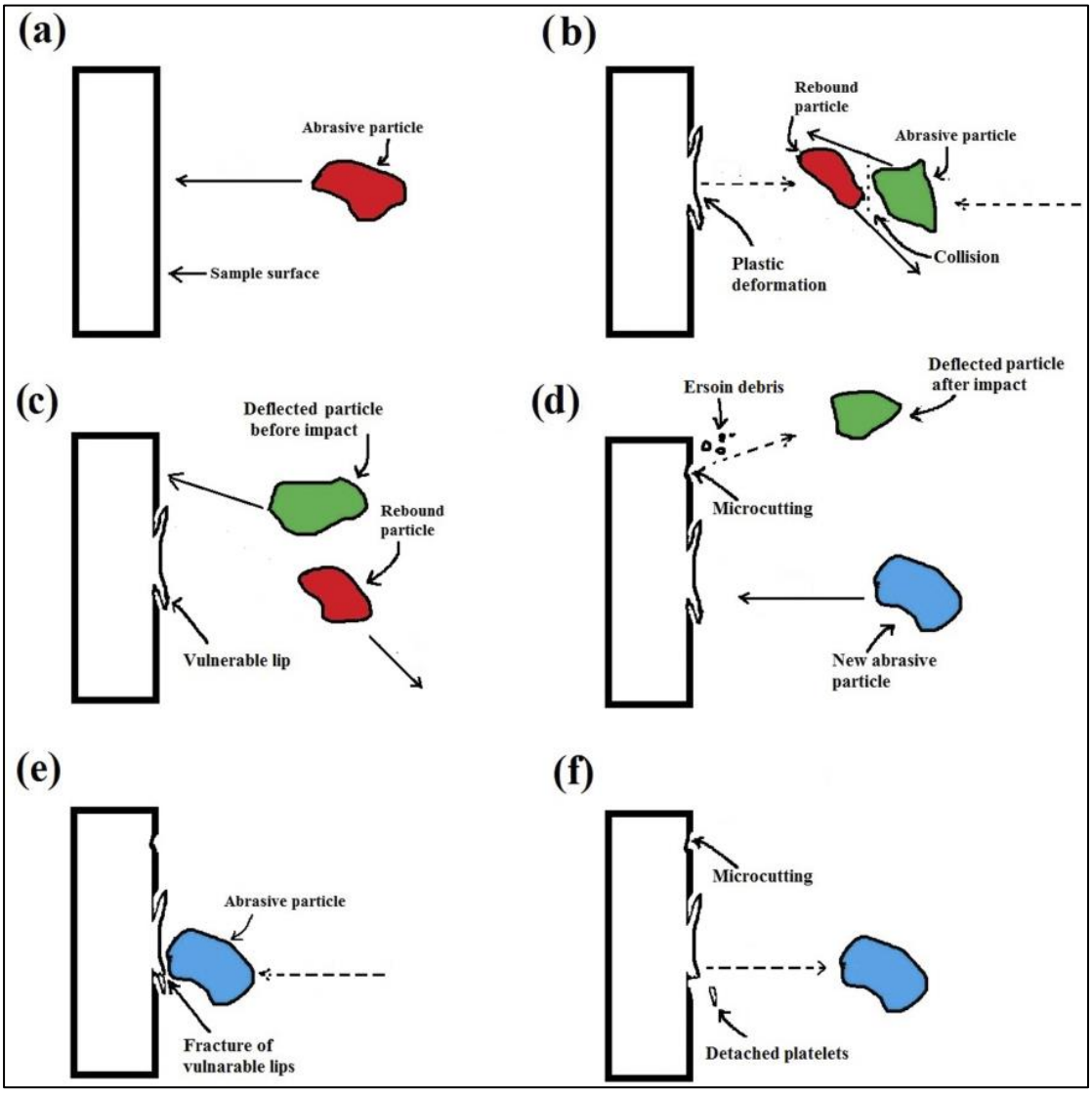

Fig. 2.6 Mechanism of slurry erosion [14]

Slurry erosion depends on both slurry and specimen characteristics. Slurry characteristics include slurry concentration, pH of slurry, size, shape, hardness, velocity and impingement angle of erodent particles. Specimen characteristics include morphology and mechanical properties (strength, hardness, ductility etc.).

Based on each parameter, a brief literature is discussed below –

2.2.1 Based on erodent particle

1. Size:

Deepak Kumar et al. [15] conducted the slurry erosion test on WC–10Co–4Cr and Al_2O_3+13TiO_2 coated turbine steel and examine the size effect of silica sand on wear rate. It was found that erosion rate increases when the particle size increased from 100 µm to 300 µm. The reason behind this increment is the increase in kinetic energy of impinging sand particles.

B.K. Gandhi et al. [16] evaluated the effect of erodent size on the slurry erosion rate of cast iron. Erodent sizes for four different experiments were 112, 225, 505 and 855µm. It was observed that erosion wear rate shows a linear direct relationship with erodent particle size.

Lindgren et al. [17] studied the effect of erodent shape and size on wear rate of titanium. They used 8 different erodent materials having different shape and size. It was evaluated that erosion rate increases with large erodent size.

Ojala et al. [18] conducted the erosion test on quenched wear resistant steel in different erosive environments. It was found that large abrasives have high wear rate due to higher kinetic energy associated with them.

Lynn et al. [19] conducted the slurry erosion test on steel using silica carbide and oil slurry. Silica carbide particles size varies from 20 to 500 µm. It was observed that for larger particles (size > 100 µm), wear rate is directly related to the kinetic energy of impinging particles but this effect was not seen in case of small particles.

Iwai et al. [20] evaluated that at start of slurry test, wear rate increases with increase in erodent size but after 4-5 hours, the effect of particles having size greater than 100µm is very less than small erodents.

2. Shape:

Lindgren et al. [17] studied the effect of erodent shape and size on wear rate of titanium. They used 8 different erodent materials having different shape and size. It

was seen that spherical shape erodents causes less wear than sharp edge erodents. This happens due to deep penetration by sharp edged erodents.

Ojala et al. [18] had found that smaller and sharper abrasive particles penetrates deeply than larger and spherical particles.

Bukhaiti et al. [21] studied effect of particle size and shape on slurry erosion of AISI 5117 steel. It was found that particles having irregular shape and sharp edges penetrates more in the target material and results in more material loss.

3. Concentration:

Deepak Kumar et al. [15] conducted the slurry erosion test on WC–10Co–4Cr and Al_2O_3+13TiO_2 coated turbine steel and examine the effect of silica sand concentration on wear rate. It was found that erosion rate increases when the slurry concentration increased from 10000 to 30000 ppm.

R. Dasgupta et al. [22] discussed the effect of slurry concentration and impact velocity on erosion rate of coated low carbon steel. It was observed that increasing slurry concentration from 20 to 30% results in high wear rate but wear rate decreases at 40% for all speeds of rotation. The reason behind this is that mobility of sand particles decreases when concentration is increased to 40%.

Modi et al. [23] studied sand concentration effect on slurry erosion of steels. From the experimental findings, it was observed that increase in sand concentration from 30% to 40% leads to decrement in wear rate. This was found because mobility of sand particles decreases with increase in sand concentration. So relative motion between sand and target material decreases and as a result material loss decreases. Also if sand concentration is high then there are more chances that sand particles itself get abraded and they became round shaped which again results in less wear than irregular shaped sand particles.

4. Hardness of erodent

Lindgren et al. [17] observed that wear rate is directly related to hardness of erodent.

Bukhaiti et al. [21] evaluated that relative hardness of erodent and target material had impact on wear rate.

Aminul Islam et al. [24] investigated that due to high relative hardness between erodent (Al_2O_3) and target material (AISI 1018 steel), Al_2O_3 particles embedded in the target material and act as surface enforcement.

5. Impact Velocity:

Deepak Kumar et al. [15] conducted the slurry erosion test on WC–10Co–4Cr and Al_2O_3+13TiO_2 coated turbine steel and examine the effect of silica sand impact velocity on wear rate. It was found that erosion rate increases when the impact velocity increased from 2250 to 4500 rpm.

R. Dasgupta et al. [22] found that wear rate is increased on increasing the speed of rotation from 600 to 800 rpm but decreases remarkably at 1000 rpm. The reason behind this is that at high rpm abrasive particles don't get sufficient time to indent. So at high rpm abrasive wear dominates to erosive wear.

Lopez et al. [25] studied the effect of impact velocity and impact angle on the erosion behaviour of AISI 304 and quenched and tempered AISI 420 stainless steels. The results obtained showed a gentle degradation regime at low impact velocity (4.5 m/s), while a severe degradation regime was found for high impact velocity (8.5 m/s).

Levy [26] studied slurry erosion on various stainless steels. From experimental findings, it was found erosion loss directly increases with slurry velocity. At high impact velocity, the larger sized particles have high erosion than small size particles.

B. Yu et al. [27] studied effect of slurry velocity on erosion-corrosion behaviour of carbon steel. The test is conducted at three different velocities: 3.5, 5.5 and 8 m/s. It was found that weight loss increases with increase in velocity because with increase in velocity, surface scale was removed quickly.

5. Impingement Angle:

Bukhaitia et al. [28] investigated the effect of impact angle on slurry erosion behaviour of 1017 steel and cast iron. In case of steel, shallow ploughing at low angle less than 15º, micro-cutting and deep ploughing at 15º to 75º and extrusion at high angle are the erosion mechanisms. Erosion mechanisms in case of high-Cr white cast iron involved both plastic deformation of the ductile matrix at low impingement angle up to 45º and brittle fracture of the carbides at high impingement angle greater than

45º. Plastic deformation leads to less volume loss as compared to brittle fracture of carbides.

Laguna-Camacho et al. [29] performed erosion test on TiN coating on AISI 4140 Steel. Impact angles for test are 30˚, 45˚, 60˚ and 90˚ with a velocity of 24 m/s. Erosion rate is higher at higher angles. Cracks and craters were observed at higher angles indicating brittle fracture. Fig. 2.7 shows the variation of erosion rate with impact angle for ductile and brittle materials.

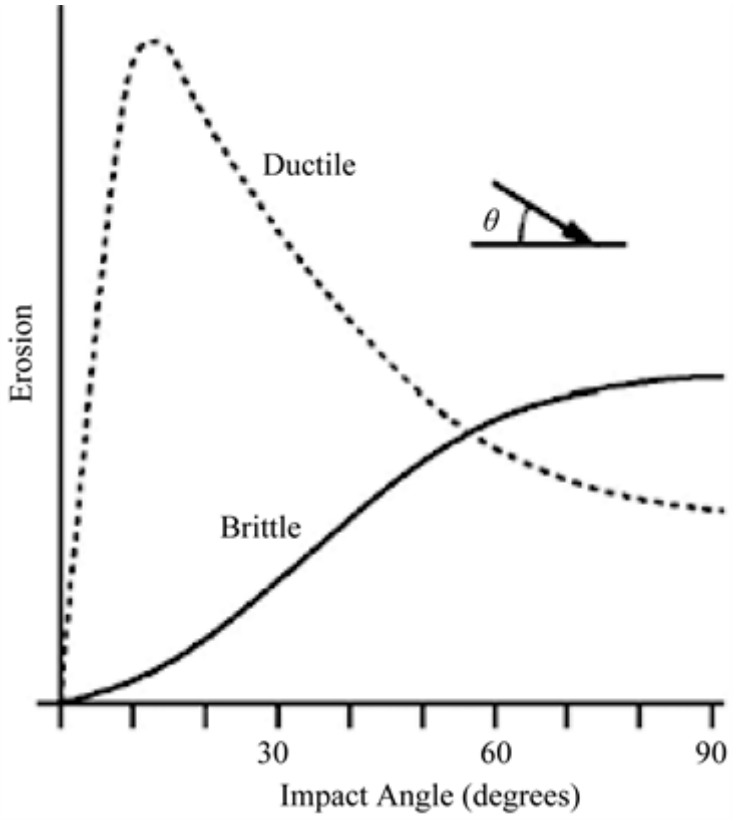

Fig. 2.7 Variation of erosion rate with impact angle for ductile and brittle materials [28]

Lopez et al. [25] studied the effect of impact velocity and impact angle on the erosion behaviour of AISI 304 and quenched and tempered AISI 420 stainless steels. The results obtained showed a gentle degradation regime at normal incidence, while a severe degradation regime was found for grazing incidence. Grooves and prows are formed at oblique impacts, while craters and indentation-like marks form at normal impact.

Burstein et al. [30] studied the effect of impingement angle on slurry erosion behaviour of stainless steel. From the experimental work, it was found that there is

high weight loss at more oblique angle of impact. Penetration and microcutting was deeper at lower angles.

Abbade et al. [31] performed sand–water slurry erosion on API 5L X65 pipe steel. After quenching from inter-critical temperature the API 5L X65 pipe steel showed slurry erosion rates increasing on the angle of attack until 30° and later decreasing until 90°. Extrusion and fracture of formed platelets were the material removal mechanism.

2.2.2 Based on target material

Morphology and mechanical properties are the two characteristics of target material that influences the slurry erosion rate. Microstructure and mechanical properties are directly related to each other.

Neeraj et al. [32] performed multi-axial forging on HSLA steel and studied the influence of this processing on slurry erosion. It was investigated that dual phase HSLA steel obtained after multi-axial forging and quenching is 1.5 times more erosion resistant than as received HSLA steel due to high toughness, hardness and greater strain hardening capacity. Simply after multi-axial forging, microstructure of HSLA steel consisted of ultrafine-grained ferrite and well dispersed fragmented pearlite, which shows improved slurry erosion resistance. Dual phase steel had ferrite and martensite as its micro-constituents in microstructure. Martensite provides high hardness and ferrite is responsible for toughness. It was observed that cumulative weight loss goes on decreasing as time of test increases. This was mainly due to progressive degradation of sand particles and secondly due to strain hardening.

Avnish et al. [33] studied effect of heat treatment on slurry erosion of cast 23-8-N nitronic steel. It was found that dissolution of carbides, formation of equiaxed grains and twins upon heating to 1220ºC and holding 150 min. results in increment of slurry erosion resistance of nitronic steel. Toughness, tensile strength and strain hardening capacity of nitronic steel were found to be increased after heat treatment.

Brij Kishor et al. [34] studied slurry erosion of 13Cr4Ni stainless steel after thermo-mechanical processing. Thermo-mechanical processing (950 °C, 0.001 s^{-1}) results in fine grain lath martensite and shows slurry erosion resistance was improved by 78% as compared to as received 13/4 martensitic steel. This is due to higher strength,

toughness, elongation and strain hardening capacity after thermo-mechanical processing.

Ankit Sharma et al. [8] performed air jet erosion test on medium carbon steel. 0.4% C normalized steel is heat treated to inter-critical region for 2, 4, and 5 min, respectively and three different dual phase structures steels were developed after quenching from inter-critical region. 5 min holding time dual phase steel had high hardness and tensile strength than other two because martensite volume fraction increased with increase in holding time. Erosive wear tests were performed at different angles (30º, 60º and 90º) and different velocities (45, 72 and 95 m/s) using silica sand (avg. size 200 µm) on air-jet erosion test rig. The results indicate that steel having high martensite volume fraction shows least erosion wear. Also dual phase structures shows less wear due to hard martensite and soft ferrite combination.

Dehsorkhi et al. [35] studied the effect of cold rolling followed by annealing on wear behaviour of AISI 304L stainless steel. Rolling process deforms the material and changes the grain size. After rolling, three different grain size materials (650 nm, 3 µm and 12 µm) were produced. Sliding wear test was performed at different loads (10 N, 20 N and 30 N) and it was found that the material having 650 nm grain size had less wear at 10 N and 20 N while high wear at 30 N load. This is due to higher martensitic formation at high load.

Sapate et al. [36] performed slurry test on En-31 bearing steel and studied effect of microstructure on wear. Quenching and tempering at various temperatures (210ºC, 300ºC, 410ºC and 550ºC) were done to change the microstructure characteristics. It was found that wear volume loss is directly related with sliding distance, slurry concentration and normal load. Volume loss varies more with normal load than slurry concentration. Volume loss decreases with increase in hardness and also decreased due to fine carbides and martensite morphology after heat treatment.

2.3 Problem formulation

Wear causes an enormous annual expenditure to industry and consumers. For some industries such as oil and gas, pipeline, hydraulic machine, agriculture, power plants, aerospace, etc., slurry erosive wear is the main wear that is responsible for failure of components. Thus the magnitude of losses caused to mankind makes it absolutely necessary to study ways to minimize it. Thus minimizing wear, affects the economics of production in a major way. The available literature suggests that the work has been done on the erosive wear of steels and thermal cycling of steels. However, the author could not find any study related to combined work on thermal cycling and erosive wear. Hence the aim of present work is to study the slurry erosive wear of thermal cycled medium carbon low alloy steel. From literature survey it is found out that slurry erosive wear mainly depends on hardness, which is directly related to microstructure and heat treatment. With thermal cycling, excellent combination of strength, hardness and toughness are obtained. Medium carbon low alloy steel is selected due to its wide range of applications in erosive environment. The objective of my study is to minimize the slurry erosive wear volume loss.

Chapter 3

Plan of work

Fig. 3.1 shows the schematic sketch of plan of work. These all processes are explained step by step in next chapter.

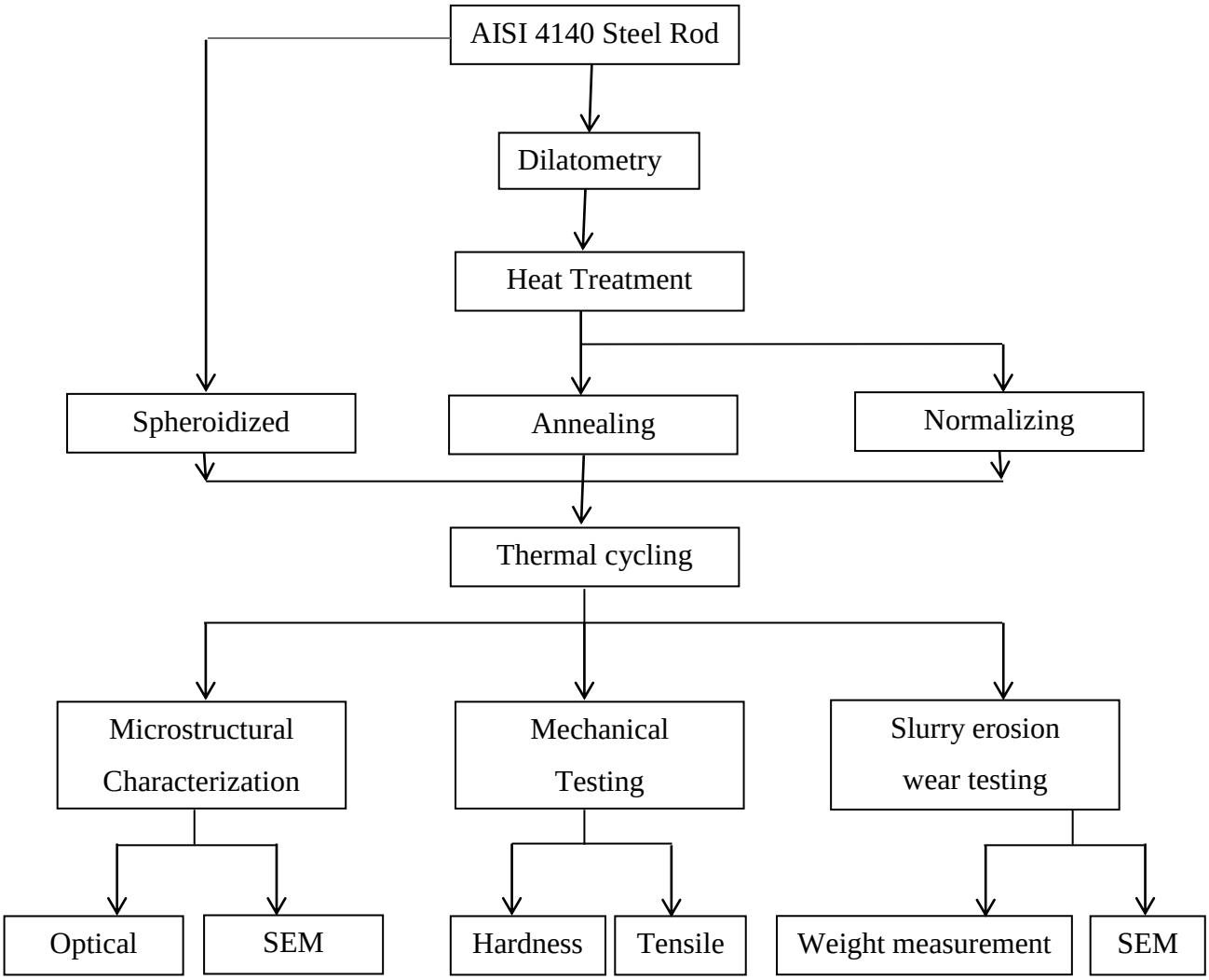

Fig. 3.1 Flow diagram of plan of work

Chapter 4

Experimental procedure

4.1 Material

Medium carbon low alloy steel was obtained in rod shape of dimension 10 mm dia. and 1000 mm long. Since we know that various alloying elements influences different properties of steel. So, it is necessary to find out the chemical composition of as-received material.

The chemical composition of as-received medium carbon low alloy steel is determined on Thermo Jarrell ash spark emission spectroscope. The obtained chemical composition is –

Table 4.1 : Chemical composition of as-received medium carbon low alloy steel

Element	**C**	**Si**	**Mn**	**P**	**S**	**Cr**	**Mo**	**Fe**
Wt. (%)	0.39	0.20	0.76	0.01	0.005	0.80	0.16	Balance

4.2 Dilatometry

Dilatometry is used to determine the A1 and A3 temperature. These are the critical temperatures as phase changes on these temperatures during heating or cooling. Dilatometry is a technique in which a dimension of a material under negligible load is measured (e.g. expansion measurement or shrinkage measurement) as a function of temperature while the substance is subjected to a controlled temperature program in a specified atmosphere. A 10 mm dia. and 70 mm long sample is cut for dilation test which is performed on Gleeble 3800. Sample is heated to 1100ºC at a heating rate of 5ºC/s.

4.3 Heat treatment

Before thermal cycling, normalization and annealing is done on as-received material i.e. in spheroidized condition, to study the effect of initial microstructure on thermal cycling and slurry erosion. Heat treatment is done on rectangular vertical electric furnace. Fig. 4.1 shows schematic representation of normalization and annealing heat treatment.

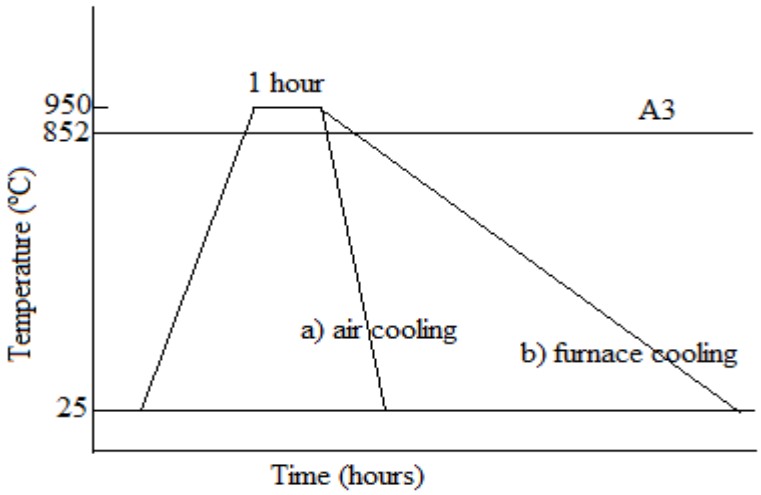

Fig. 4.1 Heat treatment a) normalizing b) annealing

4.4 Thermal cycling

After normalizing and annealing, samples are machined before doing thermal cycling. Machining is done because scaling and decarburization occur at surface as there was no protective environment used during heat treatment. Fig. 4.2 shows the applied thermal cycling in this work. Thermal cycling consisted of cyclic heating and cooling at 50ºC above (902ºC) and below (802ºC) A3 temperature followed by forced air cooling to room temperature.

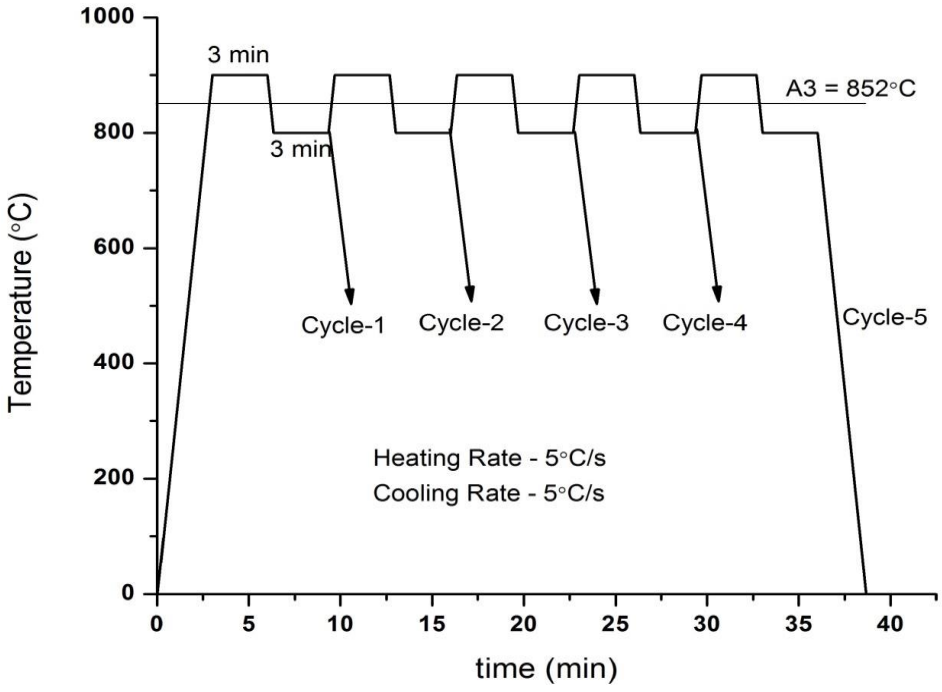

Fig. 4.2 Thermal cycling

Spheroidized, Annealed and Normalized samples of size dia. 10mm and 80mm long are fitted one by one on copper grips in heating chamber of thermo-mechanical simulator (Gleeble-3800) shown in Fig. 4.3(a). Only 10mm long sample was subjected to uniform thermal cycling shown in Fig. 4.3(b). Other part of sample was covered with copper grips because of limitation of thermal gradient occurrence in large part. Thermal cycling is executed through a program.

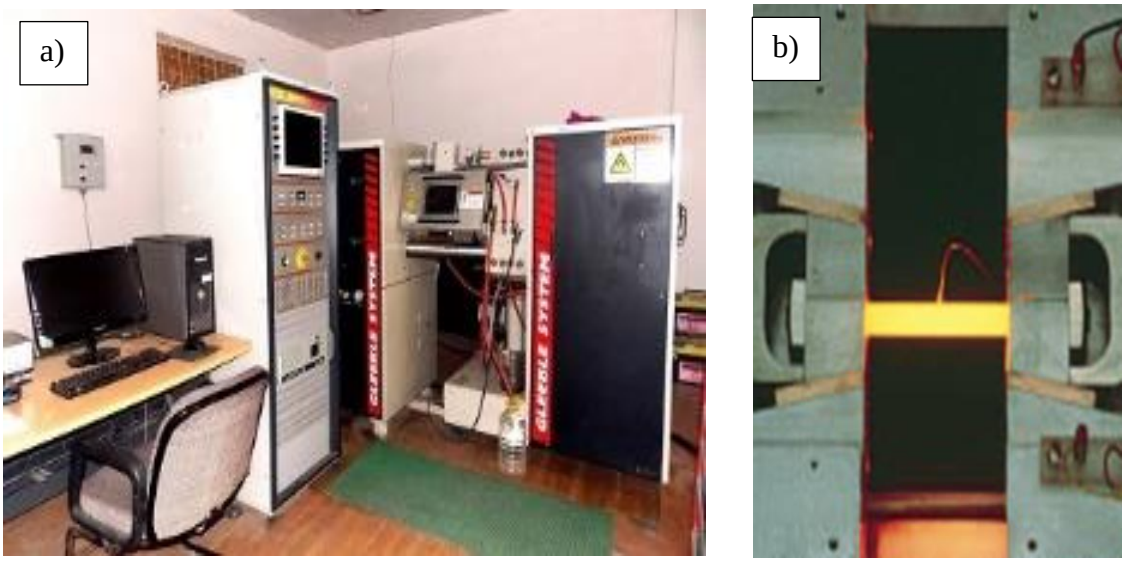

Fig. 4.3 a) Thermo-mechanical simulator Gleeble 3800; b) Heating chamber of Gleeble 3800

The Gleeble 3800 impressive heating rates and compression tension forces enable researchers to develop new steel processing methods and quantify performance characteristics.

Maximum stroke rate - 2000mm/sec

Maximum heating/quenching rate - 10,000ºC/sec

Maximum specimen size – 20mm diameter

APPLICATIONS: Compression test, Thermal/mechanical fatigue, Weld HAZ simulation, CCT/TTT curve, Thermal cycling, Heat treatment, Dilatometry, and many more applications.

LIMITATION: Only conducting materials can be tested.

4.5 Sample Preparation

Thermal cycled samples (10mm long) are cut on Isomet 4000 diamond cutter shown in Fig. 4.4, which are used further for microstructure, hardness and slurry erosion testing.

Fig. 4.4 Isomet 4000 diamond cutter

For microstructural and hardness investigation, first the samples are polished on belt to remove deeper scratches and also for flattening of samples. Now polishing is done on 320, 800, 1200 and 1500 grit size emery papers respectively. On every successive paper the sample is rotated by 90º so that previous paper scratches are abraded. Last step of polishing is cloth polishing. Velvet cloth is being put on wheel and alumina slurry is sprayed continuously on cloth during polishing. Fig. 4.5 shows the cloth polisher machine, whose rpm is generally set to 200-250 for effective polishing.

Fig. 4.5 Cloth polisher machine

4.6 Optical Microscope

Polished samples are etched with 2% Nital to reveal various phases. Fig. 4.6 shows the image of optical microscope (Leica DMI 5000M) which is used to capture the microstructures of thermal cycles samples.

Fig. 4.6 Optical microscope having magnification up to 100X

4.7 Mechanical Testing

Hardness is measured at 10kg load and 15 sec. dwell time on Vickers hardness tester model number VM 50 which is shown in Fig. 4.7.

Fig. 4.7 Vickers hardness testing machine

As only (8-10) mm long part is uniformly thermal cycled on Gleeble 3800. So notch-type tensile samples are prepared to find out ultimate tensile strength. Such notch tensile samples often used to find out strength of HAZ microstructures [37]–[39]. Dimensions of notch-type tensile sample are shown in Fig. 4.8(b). Fig. 4.8(a) shows Universal testing machine model Instron 8802, which is used to perform tensile testing at strain rate of 1 mm/min.

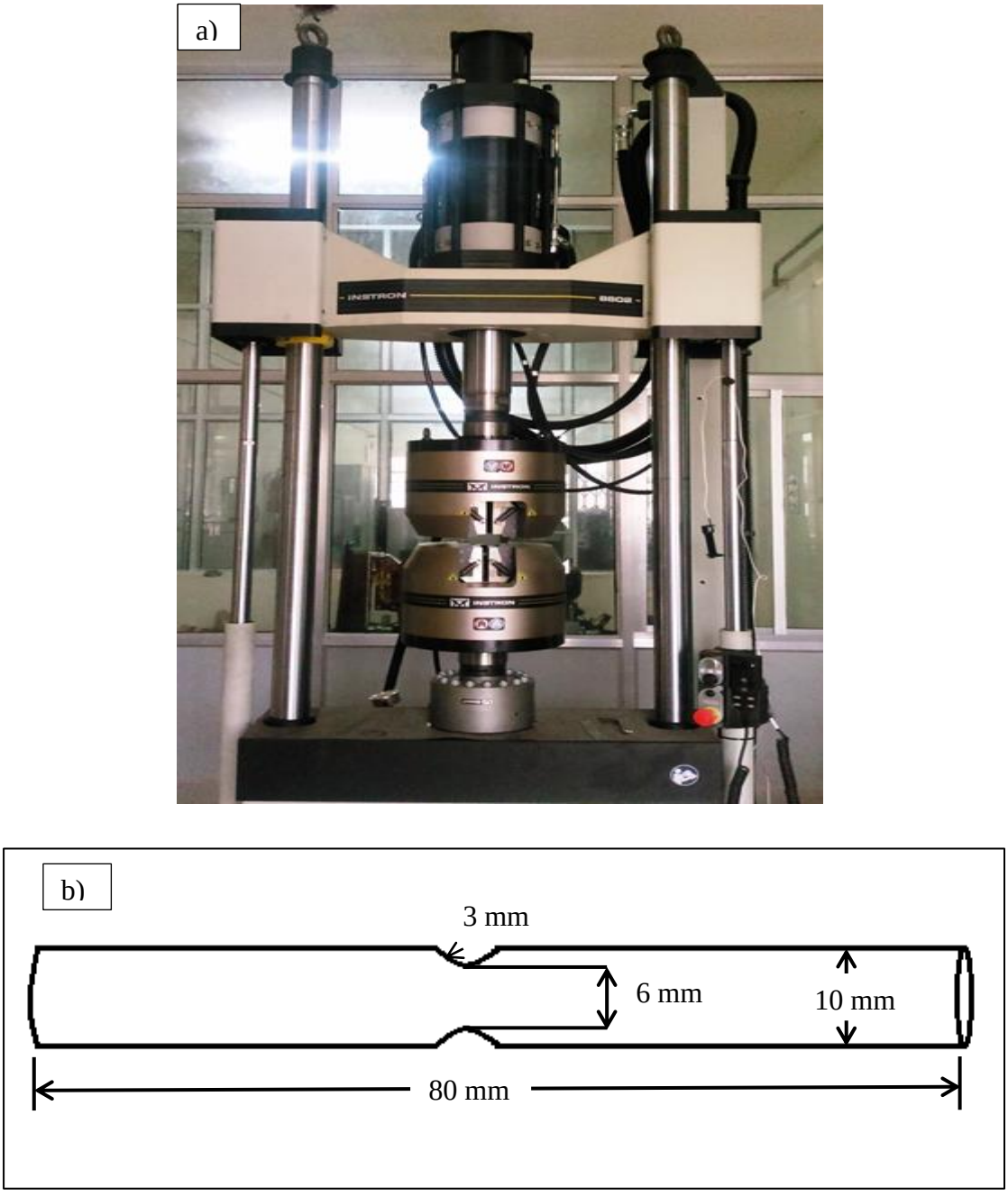

Fig. 4.8 a) Universal testing machine, b) Notch tensile sample dimension

4.8 Slurry erosion testing

Sand sieving is done sieve shaker machine shown in Fig. 4.9. Various sieve plates of different sizes (Tyler no. 35, 48, 65) are placed on the sieving machine. Coarser size sieve plate (Tyler no. 35) put on top. Sand between sieve plates 48 and 65 (size 300-212μm) is used to make slurry with tap water in 1:10 concentration ratio.

Fig. 4.9 Sieve shaker machine

Now samples are pasted on the sample holder of slurry erosion pot tester. Four samples can be pasted at a time. The slurry erosion pot tester has belt-pulley arrangement connected between electric motor and shaft. Shaft is connected with sample holder. Shaft is rotated at 500 rpm. Linear velocity of slurry is 3.60 m/s. Baffle plates are welded on the side of slurry pot to provide turbulence. After every 3 hours of slurry erosion testing, sample are removed from the sample holder for weight measurement. Samples are first washed with acetone and then dried with air blower followed by weight measurement on Mettler Toledo weighing machine having a sensitivity of 0.1 mg. Again samples are pasted on sample holder and test is continued for next 3 hours. Total test time for single sample is 24 hours. After completion of slurry test, surface roughness of each sample is measured on Mititoyo SJ-400 stylus profilometer. The various components of slurry erosion pot tester are shown in Fig. 4.10.

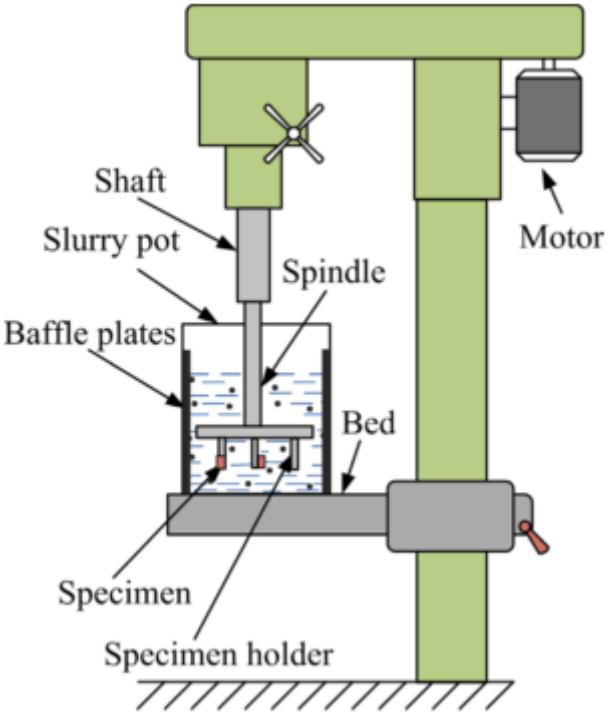

Fig. 4.10 Slurry erosion pot tester

4.9 Scanning electron microscope

High magnification morphological analysis of thermal cycling and worn out samples are done on SEM, shown in Fig. 4.11.

Fig. 4.11 Scanning electron microscope

Chapter 5

Results and Discussion

5.1 Dilatometry

A 10 mm dia. and 70 mm long sample is cut for dilation test which is performed on Gleeble 3800. Sample is heated to 1100ºC at a heating rate of 5ºC/s. Change in slope represents the phase change. From Fig. 5.1, A1 temperature is 756ºC and A3 temperature is 852ºC.

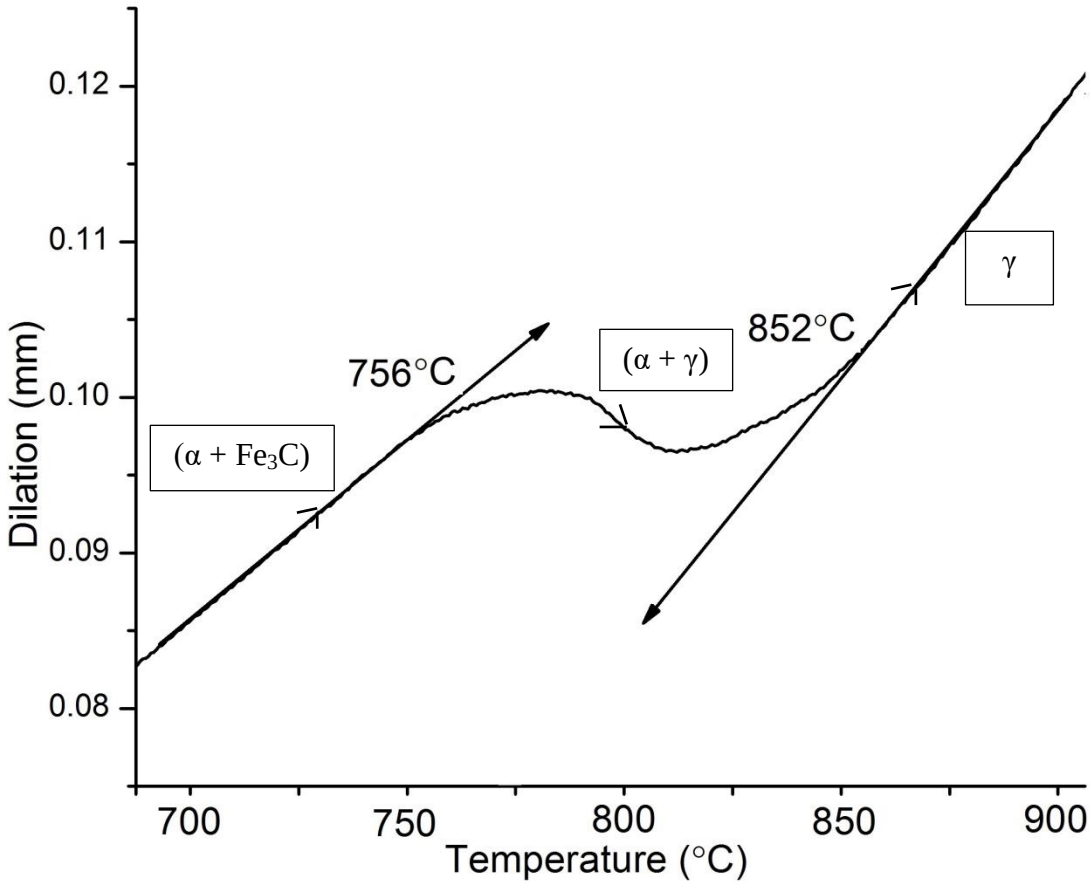

Fig. 5.1 Dilatometry curve during heating

5.2 Microstructure Evaluation

Fig. 5.2 shows the microstructure of specimen quenched from 902ºC with 3 min. holding time exhibits incomplete dissolution of cementite lamellae. Black phase is martensite which is confirmed by taking micro-hardness. Micro-hardness of black phase is 832HV.

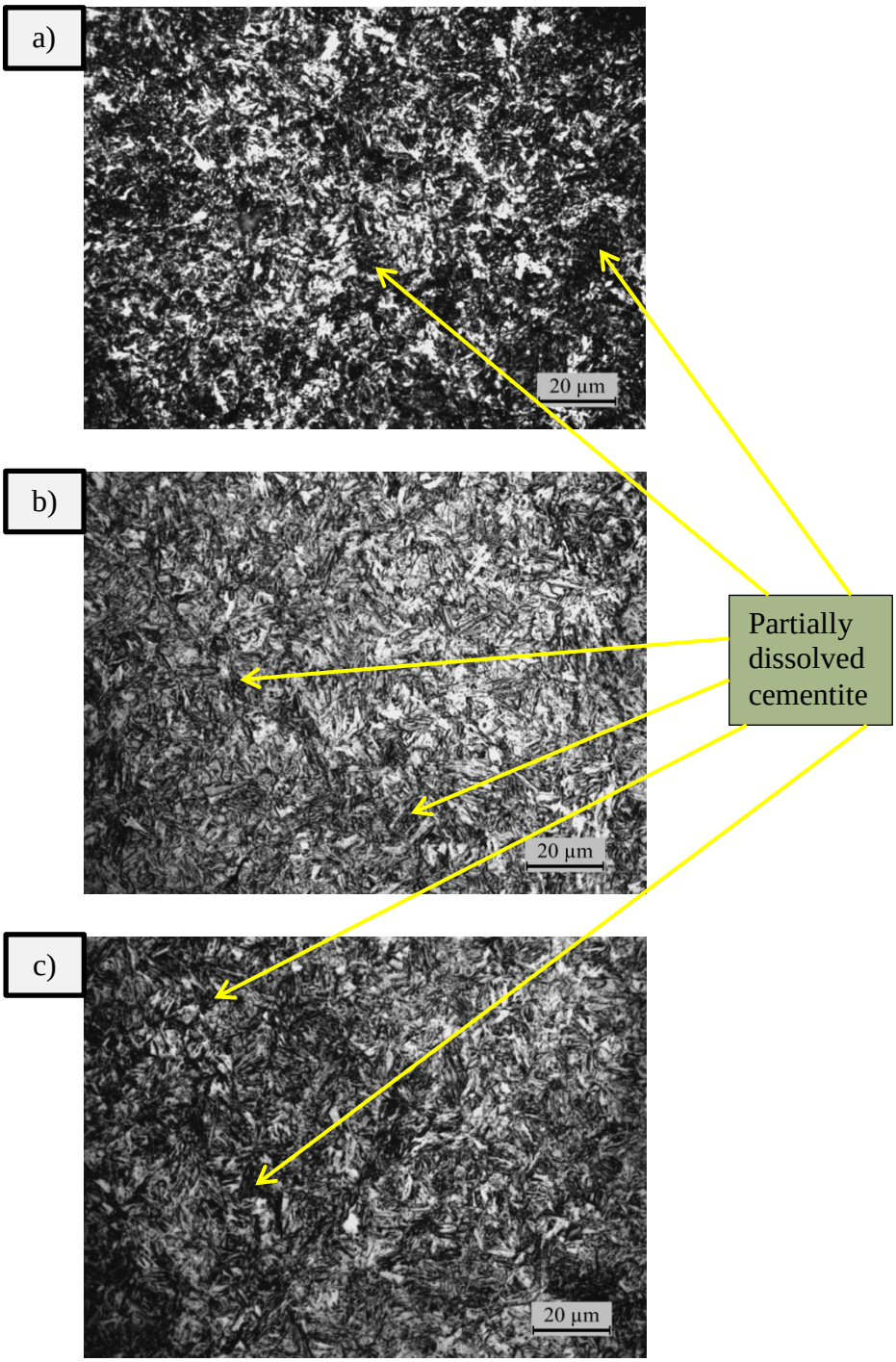

Fig. 5.2 Optical microstructure of specimen quenched from 902ºC with 3 min. holding time: a) after spheroidizing; b) after annealing and c) after normalizing

In case of spheroidized samples (Fig. 5.4 – 5.5), it is observed that after thermal cycling three changes occurs in the microstructure. Firstly, ferrite grain size reduced. Due to short holding time of 3 min. in austenite region during first thermal cycle, cementite spheroids didn't dissolve completely in the austenite matrix and this incomplete dissolution of cementite impedes the grain growth of austenite. So during cooling, fine ferrite grains formed from the fine austenite grains. Optical micrograph shown in Fig. 5.4 clears depicts ferrite grain refinement with increasing no. of thermal cycle. After first cycle, there was marginal grain size reduction upon more cycles because of previous refinement of grain. Secondly, small cementite spheroids combine and forms large cementite spheroids as shown in Fig. 5.5. Grain boundary of undissolved cementite acts as diffusion site for the already dissolved cementite in austenite matrix during cooling and this phenomenon leads to increment of cementite spheroids size [1]. Lastly, at some regions dissolution of cementite spheroids leads to high carbon region in austenite matrix and cooling leads to normal eutectoid reaction or formation of pearlite.

Fig. 5.3 shows the dissolution of cementite lamellae during austenitization. Cementite lamellae dissoltuion is diffusional transformation process. It takes time to completely dissolve but in my study holding time during austenization is very short, so complete dissolution of cementite lamellae does not occur. This impedes the grain growth of austenite and upon fast cooling, fine ferrite grain microstructure is obtained from fine austenite grains.

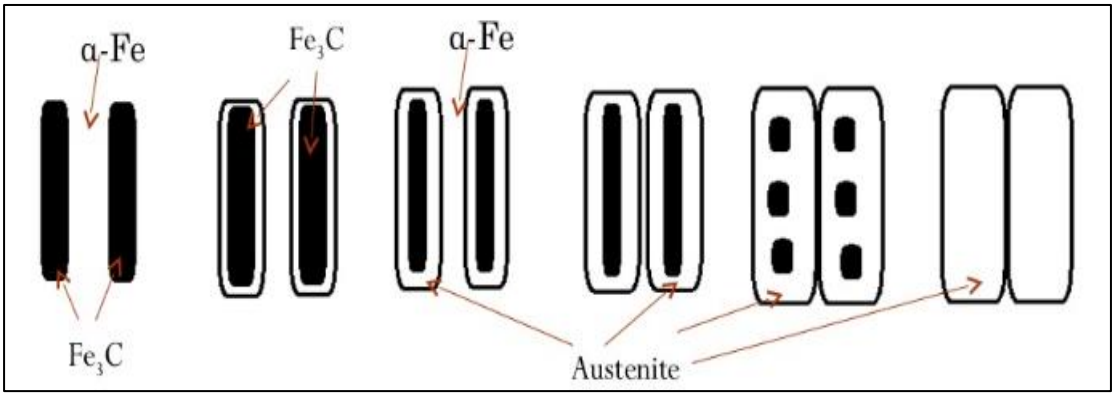

Fig. 5.3 Dissolution process during austenitization

In case of annealed samples during heating to 902ºC, ferrite changes to austenite rapidly as it is a diffusionless massive polymorphic transformation and cementite dissolves very slowly as it is diffusion controlled process [3]. Initial structure of annealed sample contains pro-eutectoid ferrite and pearlite as shown in Fig. 5.6(a). So, the region where cementite dissolves is high carbon austenite region or the pearlite region is high carbon austenite region and pro-eutectoid region is carbon-devoid austenite region. During cooling second region quickly transforms to ferrite and fine pearlite with fragmented cementite lamellae generated from the first region. Fragmented cementite lamellae are observed after thermal cycling shown in Fig. 5.7, this reveals that there is incomplete dissolution of cementite during short duration holding at 902ºC (3 min.) and 802ºC (3 min.). This incomplete dissolution of cementite lamellae is responsible for grain refinement. Non-equilibrium fast cooling also aids fragmentation of cementite lamellae. With increase in thermal cycles, fragmented cementite lamellae proportion increases and due to diffusion of carbon from adjacent lamellar faults to broken cementite leads to formation of cementite spheroids. Due to high processing temperature, fragmentation and diffusion processes occurs very fast. High processing temperature, incomplete cementite dissolution and fast cooling rate are three factors responsible for spheroidization [1].

In case of normalized samples, microstructural observations are similar to that of annealed samples that are fragmentation of cementite lamellae after thermal cycling and cementite spheroids formation after 4^{th} cycle. Normalized and annealed microstructures after thermal cycling are nearly same due to similar initial morphology of both materials except grain size. Also pearlite phase fraction goes on decreasing with increasing thermal cycles in both annealed and normalized samples.

SEM images clearly depict coarsening of cementite spheroids in case of spheroidized samples and fragmentation of cementite lamellae in case of annealed and normalized samples.

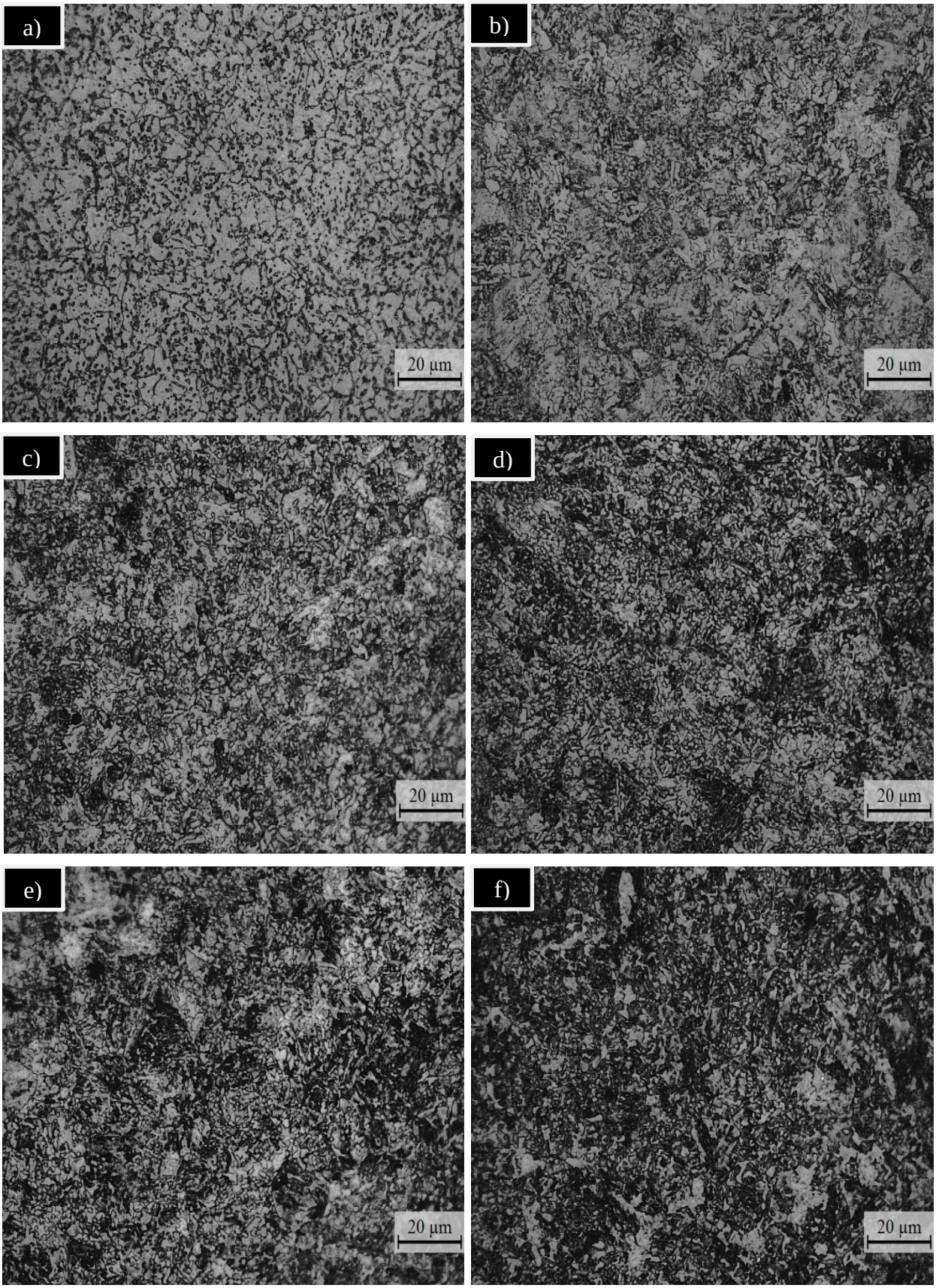

Fig. 5.4 Optical microstructure of spheroidized base and thermal cycle samples: a) base(0-cycle); b) 1-cycle; c) 2-cycle; d) 3-cycle; e) 4-cycle; and f) 5-cycle

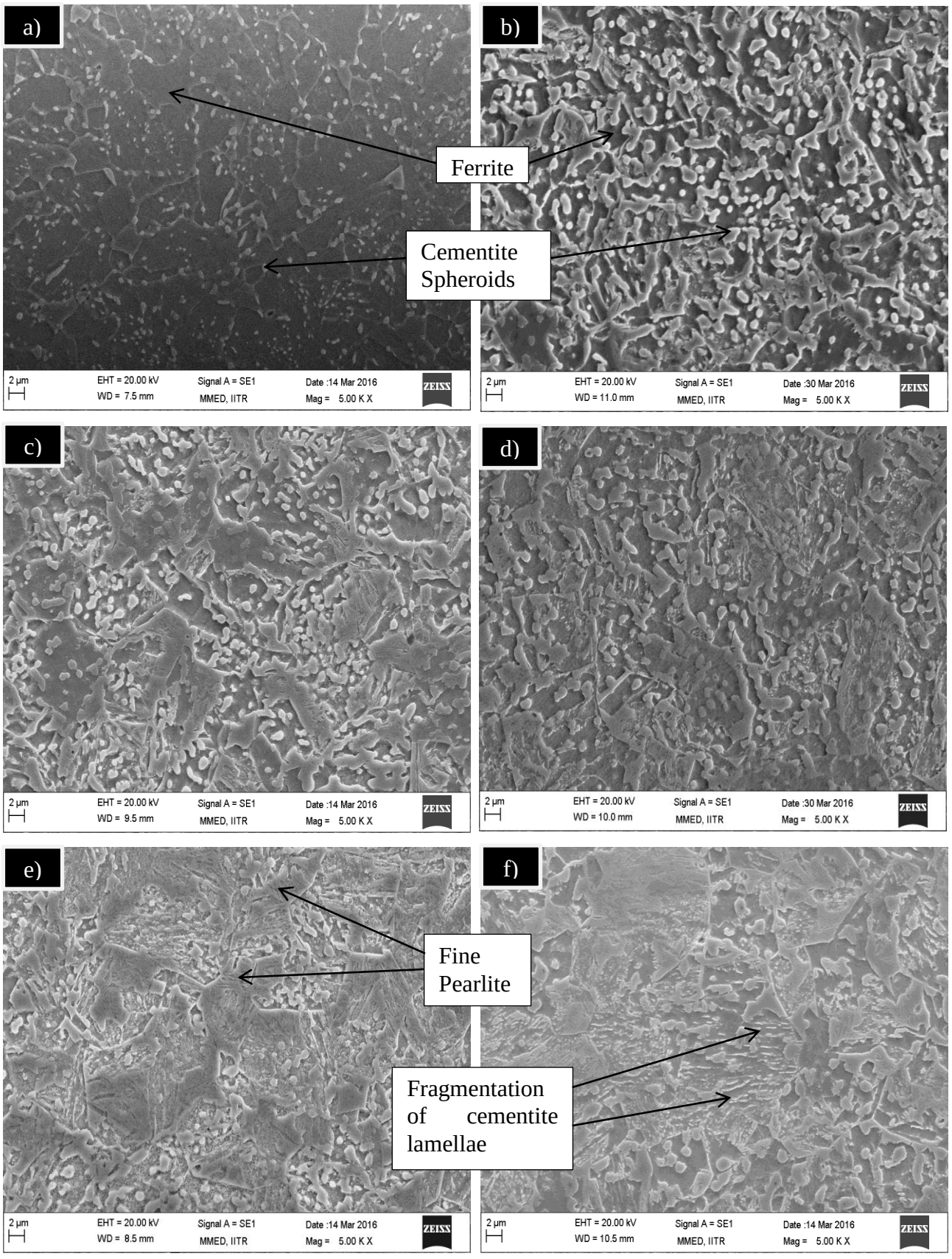

Fig. 5.5 SEM secondary electron images of spheroidized base and thermal cycle samples: a) base; b) 1-cycle; c) 2-cycle; d) 3-cycle; e) 4-cycle; and f) 5-cycle

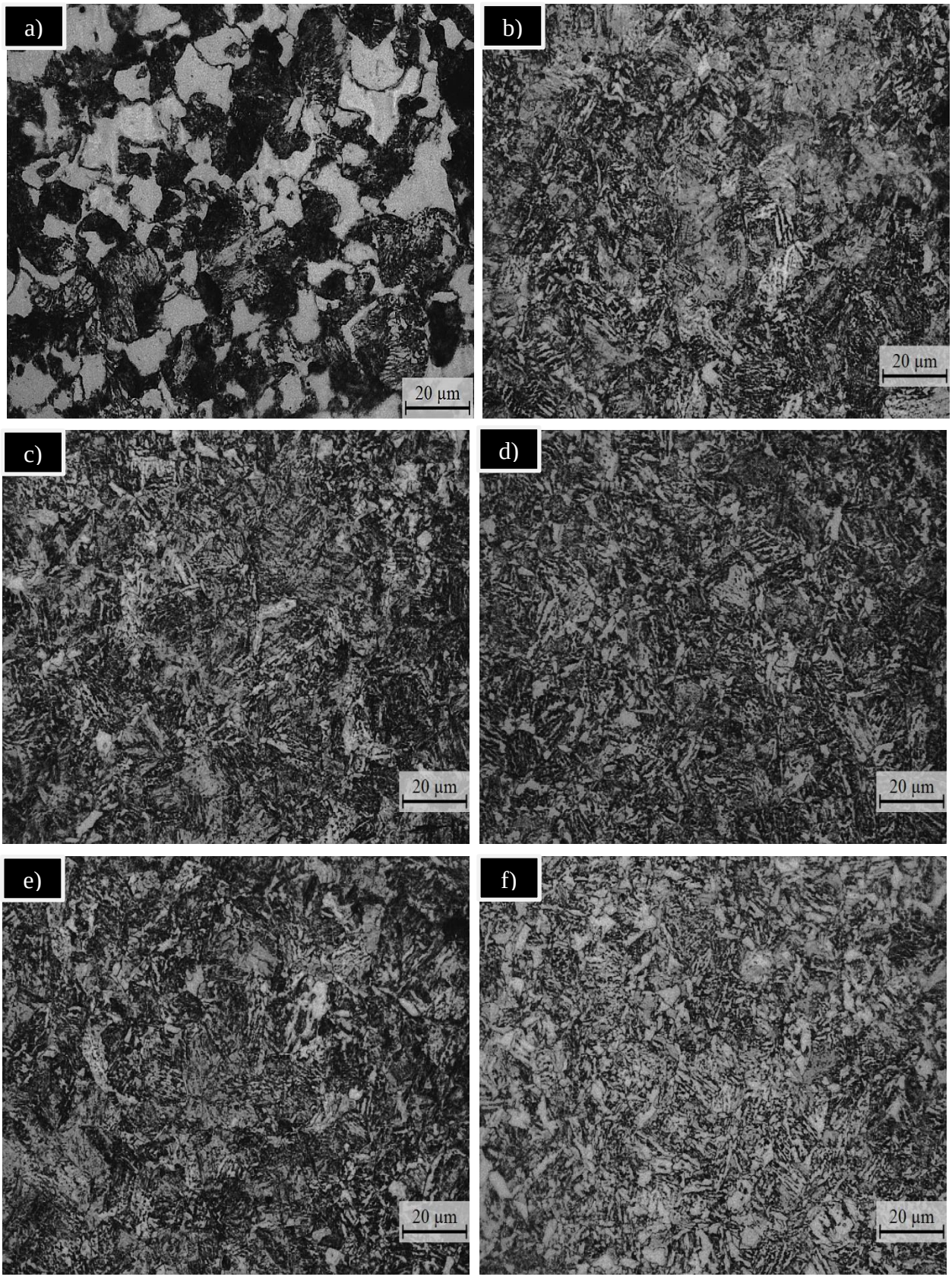

Fig. 5.6 Optical microstructure of annealed base and thermal cycle samples: a) base; b) 1-cycle; c) 2-cycle; d) 3-cycle; e) 4-cycle; and f) 5-cycle

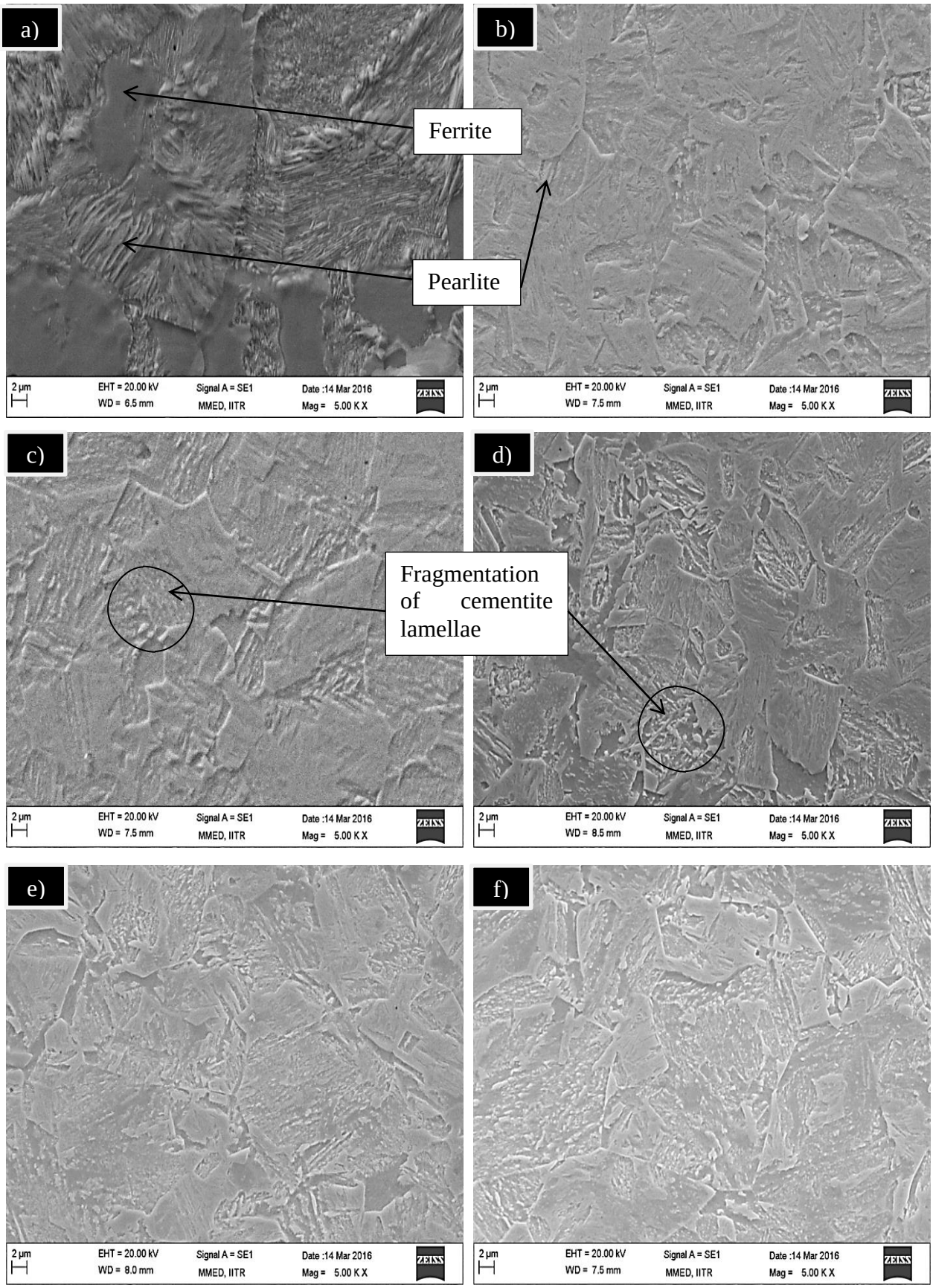

Fig. 5.7 SEM images of annealed base and thermal cycle samples: a) base; b) 1-cycle; c) 2-cycle; d) 3-cycle; e) 4-cycle; and f) 5-cycle

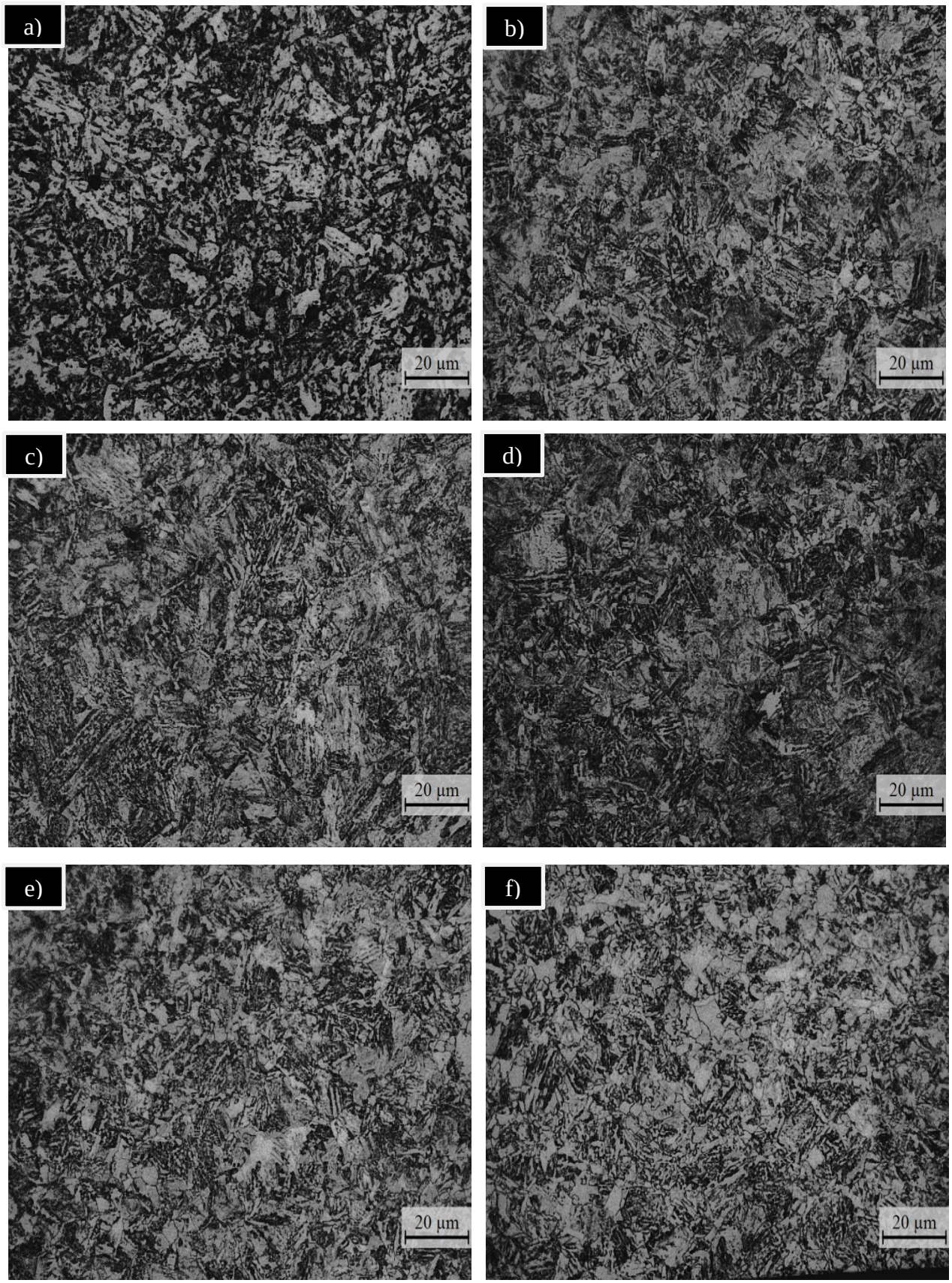

Fig. 5.8 Optical microstructure of normalized base and thermal cycle samples: a) base; b) 1-cycle; c) 2-cycle; d) 3-cycle; e) 4-cycle; and f) 5-cycle

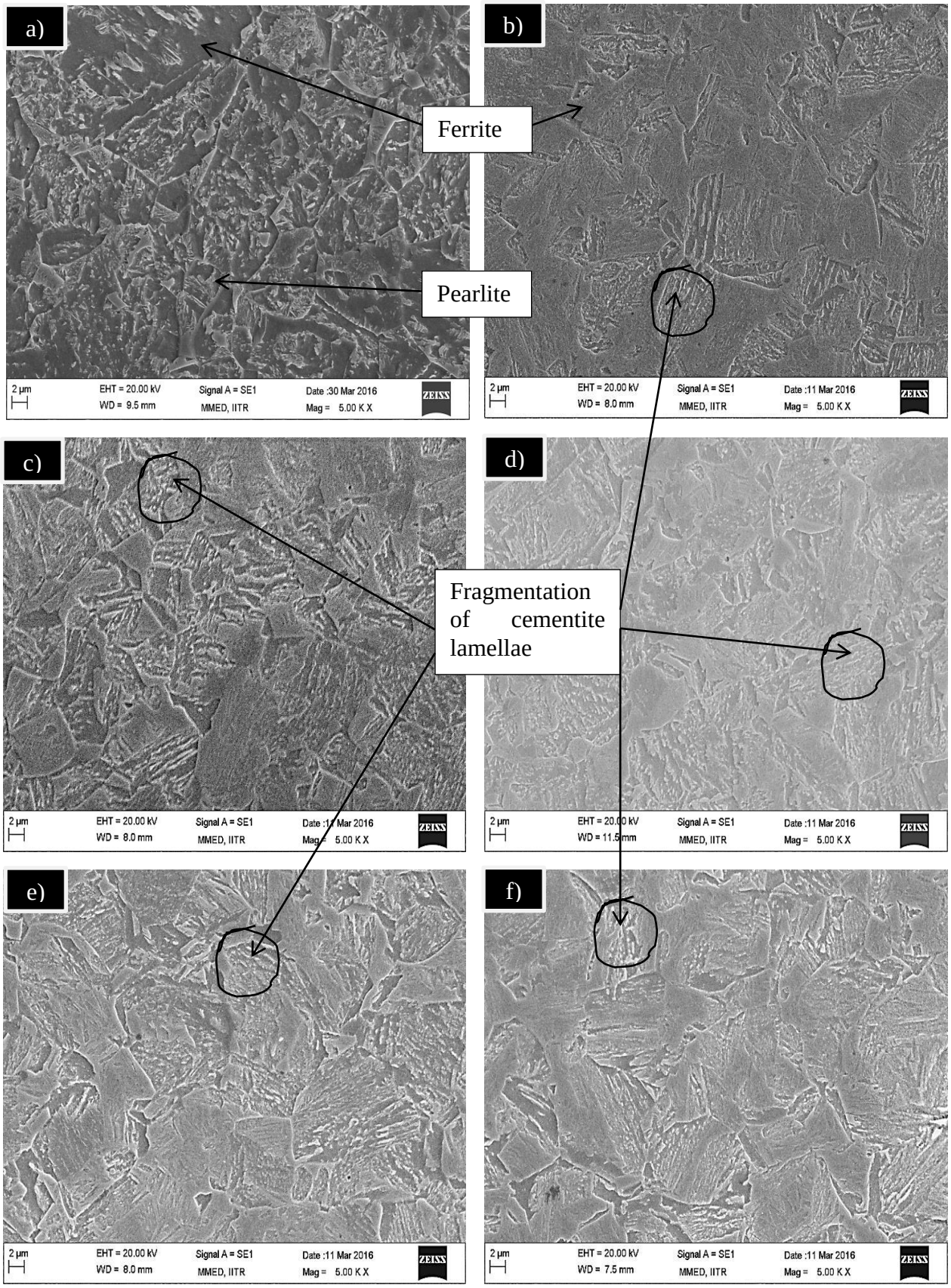

Fig. 5.9 SEM images of normalized base and thermal cycle samples: a) base; b) 1-cycle; c) 2-cycle; d) 3-cycle; e) 4-cycle; and f) 5-cycle

5.3 Mechanical properties

Fig. 5.10 shows the variation of ultimate tensile strength with increasing number of thermal cycles. Values of ultimate tensile strength with thermal cycles are given in Table 5.1. Ultimate tensile strength and hardness of spheroidized material goes on increasing with increasing number of thermal cycle. This is due to grain size reduction of ferrite matrix and formation of pearlite with increasing no. of thermal cycles. In case of annealed material, the ultimate tensile strength and hardness first increased up to 2^{nd} cycle due to grain size reduction of ferrite and pearlite then marginally decreases with increasing number of cycles due to decreased pearlite phase fraction, increased cementite fragmentation and nucleation of cementite spheroids. Similar variation is seen in normalized material and the reason is same as to that of annealed case.

Table 5.1 : Ultimate tensile strength of thermal cycled samples

Material →	Ultimate Tensile Strength (MPa)		
No. of cycles ↓	Spheroidized	Annealed	Normalized
0	970	579	1208
1	1186	1747	1635
2	1342	1860	1688
3	1450	1802	1699
4	1486	1803	1668
5	1493	1790	1659

Increment in ultimate tensile strength –

Spheroidized – 1493 MPa after 5^{th} cycle – 53.9% increase

Annealed – 1860 MPa after 2^{nd} cycle – 221.2% increase

Normalized – 1699 after 3^{rd} cycle – 40.6% increase

Maximum effect is found in thermal cycling on annealed material. This is due to higher thermal cycling effect on initial coarse grain material as compared to fine grain material [13].

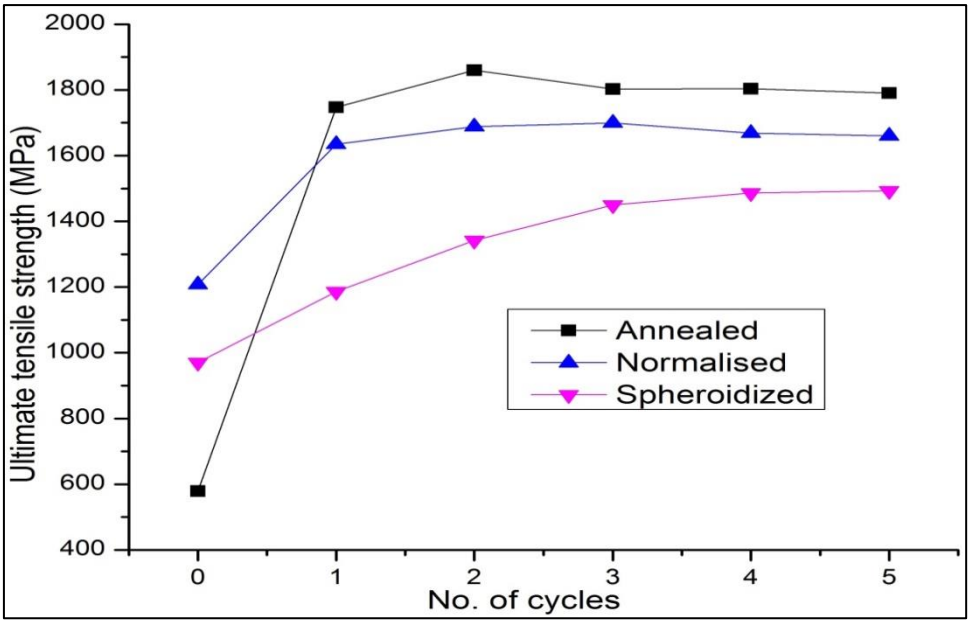

Fig. 5.10 Variation of ultimate tensile strength of different materials with thermal cycles

Fig. 5.11 shows variation of hardness with thermal cycles for spheroidized, annealed and normalized materials. Hardness and ultimate tensile strength shows similar variation as both are similar properties with different deformation mechanism. It is observed that hardness values increased after slurry erosion test. This is due to the strain hardening by the continuously impact of sand particles. Values of hardness (before and after slurry erosion) at different no. of thermal cycle are given in Table 5.2.

Table 5.2 : Vickers hardness values of different materials after various thermal cycles

No. of cycles	Vickers Hardness (HV) (Load-10kg Dwell time-15sec)					
	Spheroidized		Annealed		Normalized	
	Before Erosion	After Erosion	Before Erosion	After Erosion	Before Erosion	After Erosion
0	234 ± 5	238 ± 5	175 ± 4	180 ± 5	296 ± 6	308 ± 5
1	313 ± 6	340 ± 5	413 ± 5	420 ± 4	404 ± 5	416 ± 6
2	339 ± 5	360 ± 8	436 ± 6	450 ± 5	421 ± 7	430 ± 5
3	355 ± 7	382 ± 7	432 ± 7	441 ± 7	425 ± 8	437 ± 7
4	373 ± 8	398 ± 6	427 ± 6	445 ± 7	419 ± 6	425 ± 8
5	383 ± 6	405 ± 6	424 ± 6	441 ± 7	409 ± 5	417 ± 6

Increment in Hardness after thermal cycling –

Spheroidized – 383 HV after 5th cycle – 63.67% increase

Annealed – 436 HV after 2nd cycle – 149.14% increase

Normalized – 425 HV after 3rd cycle – 43.58% increase

Hardness increases due to grain refinement.

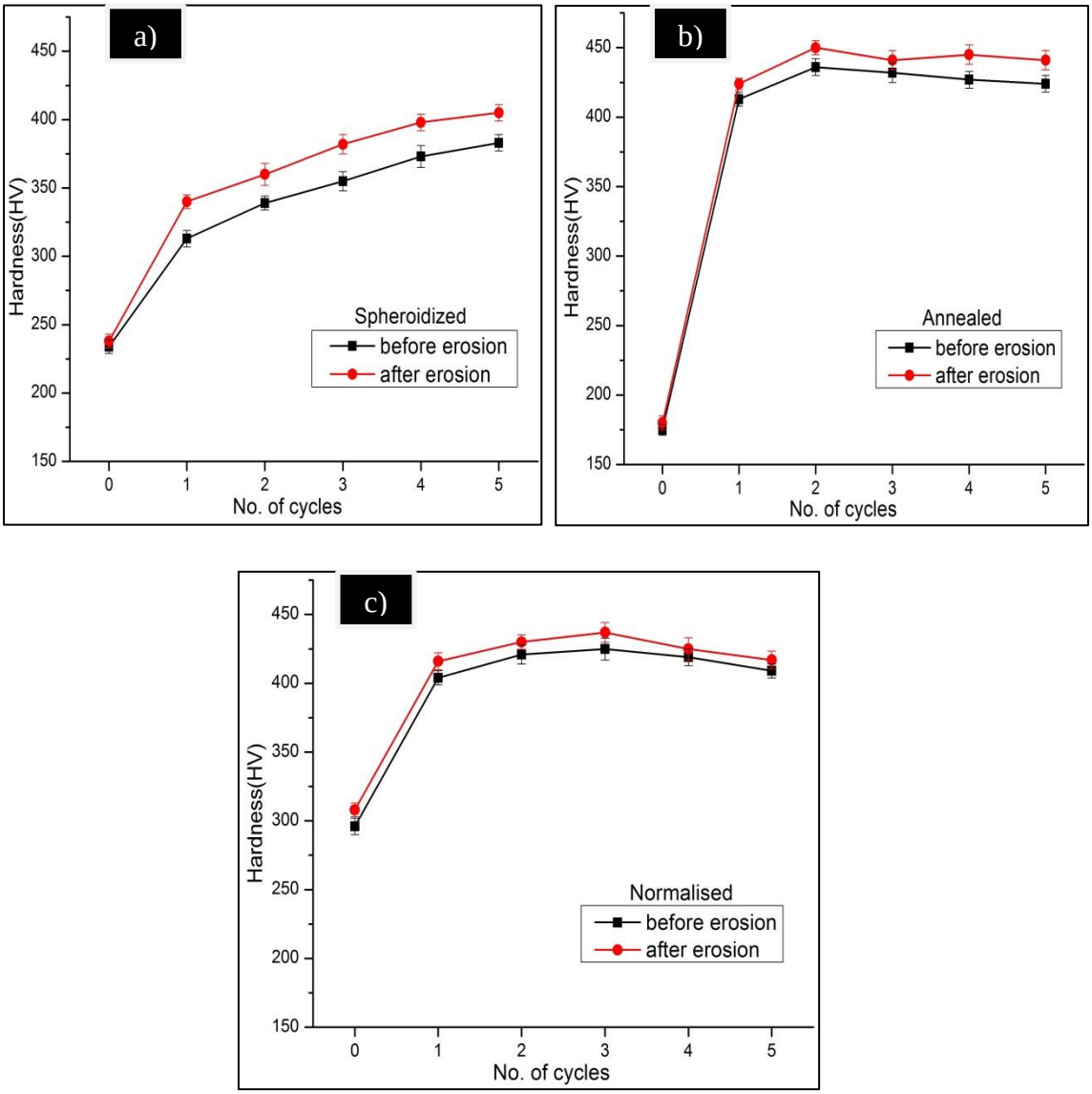

Fig. 5.11 Variation of hardness with thermal cycles before and after erosion: a) Spheroidized; b) Annealed; and c) Normalized samples

5.4 Slurry erosion results

Initial dimensions of all samples before slurry erosion are summarized in Table 5.3.

Table 5.3 : Initial dimensions of all steel samples

Sample / Thermal cycle ↓		Diameter (mm)	Height (mm)	Surface area exposed to slurry erosion (mm^2)	Weight (mg)
Spheroidized	0	8.85	6.00	228.33	2802.4
	1	9.13	4.70	200.27	2276.8
	2	9.26	4.52	198.83	2265.3
	3	9.13	4.84	204.29	2449.6
	4	9.06	3.79	172.34	1834.5
	5	9.20	3.64	171.68	1844.1
Annealed	0	8.93	4.93	200.94	2320.1
	1	9.16	3.60	169.49	1791.3
	2	9.04	2.97	148.53	1428.3
	3	9.09	3.62	168.27	1688.5
	4	9.07	3.24	156.93	1572.8
	5	9.17	2.74	144.97	1368.1
Normalized	0	8.84	2.83	139.97	1343.1
	1	8.98	2.20	125.40	1062.9
	2	9.22	2.26	132.22	1139.0
	3	9.08	3.11	153.46	1498.1
	4	9.00	2.73	140.80	1301.1
	5	9.06	3.12	153.27	1537.3

Weights of each sample after every 3 hours of slurry erosion testing are summarized in Table 5.4.

Table 1.4 : Weight measurement after slurry erosion test

Sample	Thermal cycle ↓	Weight (mg)							
		3hr	6hr	9hr	12hr	15hr	18hr	21hr	24hr
Spheroidized	0	2797.8	2793.7	2790.2	2787.3	2785.0	2782.9	2781.0	2779.2
	1	2272.4	2270.1	2268.5	2267.3	2266.2	2264.8	2263.7	2263.0
	2	2261.5	2258.8	2257.4	2256.4	2255.5	2254.7	2253.8	2253.1
	3	2445.7	2443.4	2441.6	2440.9	2439.9	2439.3	2438.6	2438.0
	4	1831.5	1829.2	1828.2	1827.7	1827.2	1826.1	1825.7	1825.2
	5	1841.5	1839.7	1838.2	1837.7	1836.7	1836.0	1835.4	1835.1
Annealed	0	2316.3	2313.2	2310.8	2309.2	2307.6	2306.2	2304.8	2303.3
	1	1788.8	1786.6	1785.6	1784.8	1784.1	1783.5	1783.1	1782.9
	2	1426.6	1425.3	1424.3	1423.6	1423.0	1422.5	1422.1	1421.9
	3	1686.7	1685.4	1684.0	1683.0	1682.3	1681.7	1681.3	1681.0
	4	1570.8	1569.4	1568.3	1567.4	1566.8	1566.4	1566.0	1565.8
	5	1366.3	1365.0	1364.0	1363.2	1362.6	1362.1	1361.7	1361.5
Normalized	0	1340.3	1338.7	1337.4	1336.3	1335.2	1334.2	1333.8	1333.3
	1	1060.8	1059.4	1058.7	1058.1	1057.6	1057.1	1056.8	1056.6
	2	1137.4	1136.1	1135.2	1134.3	1133.8	1133.4	1133.1	1132.9
	3	1496.4	1494.9	1493.8	1493.0	1492.2	1491.6	1491.3	1491.1
	4	1299.4	1298.0	1297.0	1296.1	1295.5	1295.1	1294.8	1294.6
	5	1534.9	1533.1	1532.3	1531.4	1530.8	1530.3	1529.9	1529.7

Cumulative weight loss (mg/mm^2) measured after every 3 hours of slurry erosion test on spheroidized thermal-cycled samples is summarized in Table 5.5 and plotted in Fig. 5.12.

Table 5.5 : Cumulative weight loss of spheroidized base and thermal cycle samples

Material		Cumulative weight loss (mg/mm^2)							
Thermal cycle ↓		3hr	6hr	9hr	12hr	15hr	18hr	21hr	24hr
Spheroidized	0	0.0201	0.0381	0.0534	0.0661	0.0762	0.0854	0.0937	0.1016
	1	0.0193	0.0334	0.0414	0.0474	0.0529	0.0599	0.0654	0.0689
	2	0.0189	0.0322	0.0398	0.0448	0.0493	0.0530	0.0575	0.0613
	3	0.0181	0.0303	0.0391	0.0425	0.0474	0.0504	0.0538	0.0567
	4	0.0174	0.0307	0.0365	0.0394	0.0423	0.0487	0.0510	0.0539
	5	0.0151	0.0256	0.0343	0.0372	0.0431	0.0472	0.0506	0.0524

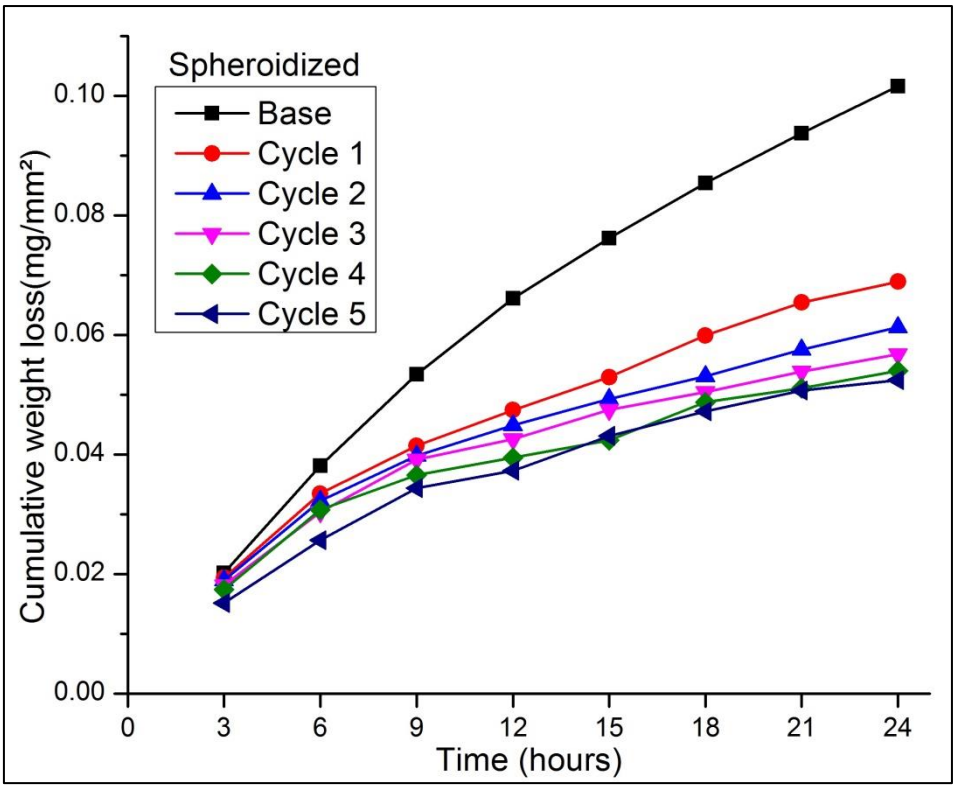

Fig. 5.12 Effect of exposure time on weight loss of spheroidized base and thermal cycle samples

Cumulative weight loss (mg/mm^2) measured after every 3 hours of slurry erosion test on annealed thermal-cycled material is summarized in Table 5.6 and plotted in Fig 5.13.

Table 5.6 : Cumulative weight loss of annealed base and thermal cycle samples

Material	Thermal cycle ↓	Cumulative weight loss (mg/mm^2)							
		3hr	6hr	9hr	12hr	15hr	18hr	21hr	24hr
Annealed	0	0.0189	0.0343	0.0462	0.0542	0.0622	0.0691	0.0761	0.0836
	1	0.0147	0.0277	0.0336	0.0383	0.0425	0.0460	0.0484	0.0495
	2	0.0121	0.0208	0.0276	0.0323	0.0363	0.0397	0.0424	0.0437
	3	0.0107	0.0184	0.0267	0.0327	0.0368	0.0404	0.0428	0.0445
	4	0.0127	0.0216	0.0287	0.0344	0.0382	0.0408	0.0433	0.0446
	5	0.0124	0.0213	0.0283	0.0338	0.0379	0.0414	0.0441	0.0455

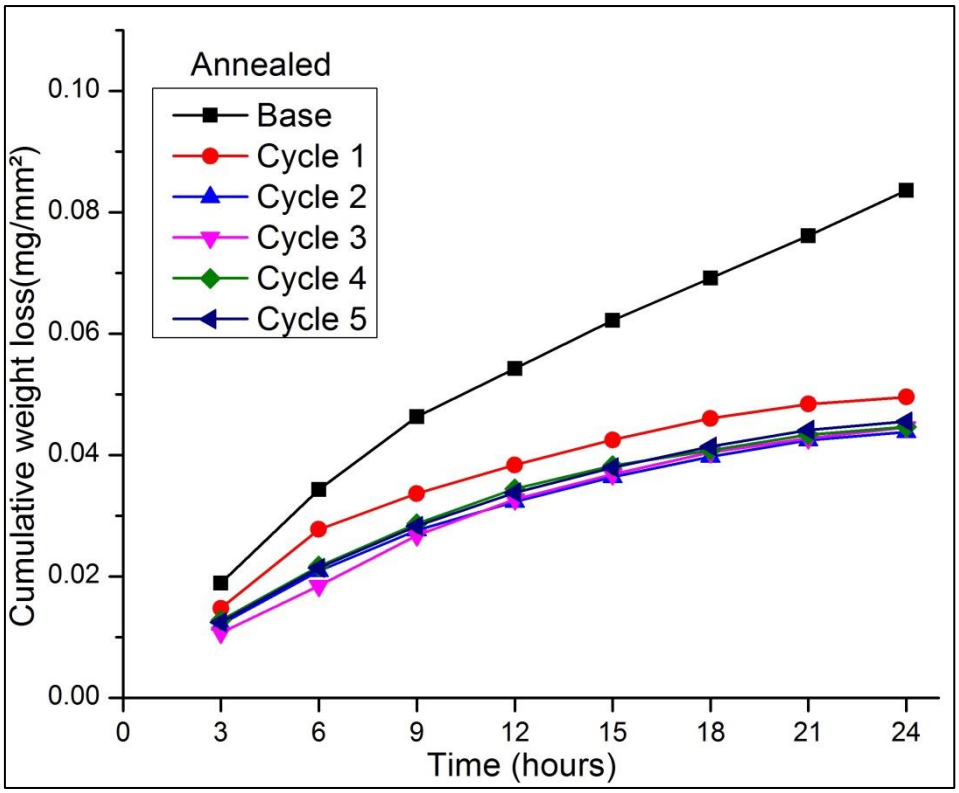

Fig. 5.13 Effect of exposure time on weight loss of annealed base and thermal cycle samples

Cumulative weight loss (mg/mm^2) measured after every 3 hours of slurry erosion test on normalized thermal-cycled material is summarized in Table 5.7 and plotted in Fig. 5.14.

Table 5.7 : Cumulative weight loss of normalized base and thermal cycle samples

Material		Cumulative weight loss (mg/mm^2)							
Thermal cycle ↓		3hr	6hr	9hr	12hr	15hr	18hr	21hr	24hr
Normalized	0	0.0200	0.0314	0.0407	0.0486	0.0564	0.0636	0.0664	0.0700
	1	0.0175	0.0287	0.0343	0.0390	0.0430	0.0470	0.0494	0.0510
	2	0.0121	0.0219	0.0287	0.0355	0.0393	0.0423	0.0446	0.0461
	3	0.0111	0.0208	0.0280	0.0332	0.0384	0.0423	0.0443	0.0456
	4	0.0120	0.0220	0.0291	0.0355	0.0397	0.0426	0.0447	0.0461
	5	0.0156	0.0274	0.0326	0.0385	0.0424	0.0456	0.0483	0.0496

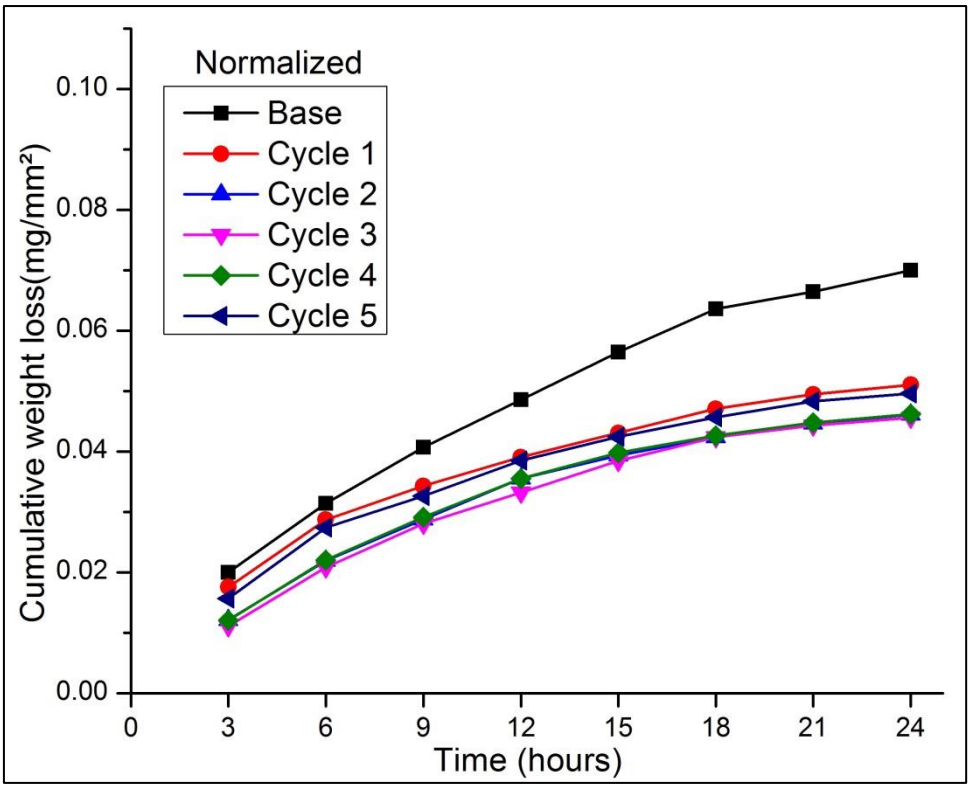

Fig. 5.14 Effect of exposure time on weight loss of normalized base and thermal cycle samples

Table 5.8 shows the percentage decrement in cumulative weight loss for all samples after thermal cycling with respect to respective base materials and spheroidized base material.

Table 5.8 : Percentage decrement in cumulative weight loss

Material / Thermal cycle ↓		Total cumulative weight loss (mg)	Percentage decrement in cumulative weight loss w.r.t. respective base material	Percentage decrement in cumulative weight loss w.r.t. spheroidized base material
Spheroidized	Base	0.1016	-	-
	Cycle 1	0.0689	32.18	32.18
	Cycle 2	0.0613	39.66	39.66
	Cycle 3	0.0567	44.19	44.19
	Cycle 4	0.0539	46.94	46.94
	Cycle 5	0.0524	48.42	48.42
Annealed	Base	0.0836	-	17.77
	Cycle 1	0.0495	40.79	51.27
	Cycle 2	0.0437	47.72	56.98
	Cycle 3	0.0445	46.77	56.20
	Cycle 4	0.0446	46.65	56.10
	Cycle 5	0.0455	45.57	55.21
Normalized	Base	0.0700	-	31.10
	Cycle 1	0.0510	27.14	49.80
	Cycle 2	0.0461	34.14	54.62
	Cycle 3	0.0456	34.85	55.11
	Cycle 4	0.0461	34.14	54.62
	Cycle 5	0.0496	29.14	51.18

For all three materials (spheroidized, annealed and normalized), thermal cycling results in reduced cumulative weight loss. Cumulative weight loss is maximum in case of spheroidized base material and minimum for annealed twice thermal cycled material. It is observed that after thermal cycling, there is reasonable good decrement

in cumulative weight loss. In all cases, material having high hardness shows minimum cumulative weight loss except spheroidized base material. Spheroidized base material has high hardness than annealed base material but cumulative weight loss of annealed base material is less than spheroidized base material. The reason is their completely different morphology. Due to fine cementite particles in ferrite base matrix in case of spheroidized base material, continuous impingement of sand particles plastically deform the ductile ferrite matrix leaving behind the hard cementite particles. These cementite particles are easily pulled out once ferrite matrix is plastically deformed. But in case of annealed base material, microstructure contains proeutectoid ferrite and pearlite. Pearlite contains alternate layers of ferrite and cementite. The erosion mechanism is same but due to better adherence between ferrite and cementite, weight loss is less as compared to spheroidized base material. Also, the cumulative weight loss curve slope with exposure time first increases steeply and after 6 hours starts decreasing and becomes nearly constant after 24 hours. This behaviour can be due to two reasons. One is the strain hardening due to continuous impact of sand particles on the sample during slurry testing. Increment in hardness values after slurry erosion test shown in Table 3 confirmed that strain hardening occurs due to impact of sand particles. Second reason is degradation of sand particles due to continuous impact on sample. Fig. 5.15 shows the SEM images of sand particles before and after slurry erosion test. SEM images depicts that there is marginal change in shape of sand particles. Size doesn't changes as hardness of sand particles is high as compared to steel samples.

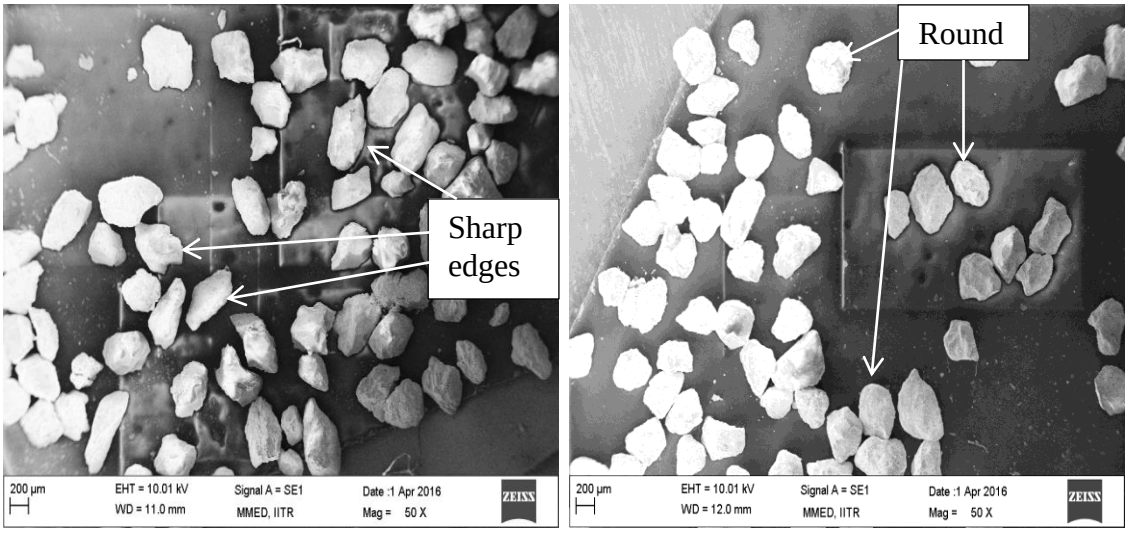

Fig. 5.15 SEM images of sand particles: a) before erosion and b) after erosion

The average slurry erosion rate is calculated as –

$$\text{Average slurry erosion rate} = \frac{\text{Total cumulative weight loss}}{\text{Density} \times \text{Exposed surface area} \times \text{Total exposure time}}$$ where,

Density of used steel = 7.85 gm/cc,

Total exposure time = 24 hour,

Cumulative weight loss and exposed surface area are different for different materials

Fig. 5.16 shows variation of average slurry erosion rate for differently processed material. Erosion rate is higher for spheroidized base material (2.36×10^{-6} $mm^3/h\ mm^2$) and it decreased by 48 % after 5^{th} thermal cycle to same material. Two cycles of thermal cycling to annealed material results in minimum erosion rate (1.01×10^{-6} $mm^3/h\ mm^2$) from all other cycles to different materials. It is found that average slurry erosion rate decreased with increase in hardness of steel similar to cumulative weight loss. Hardened AISI 1045 steel pipe shows increased erosion resistance than standard, non-hardened base material [3]. In this study, also, the slurry erosion resistance increased with increasing hardness of medium carbon low alloy steel.

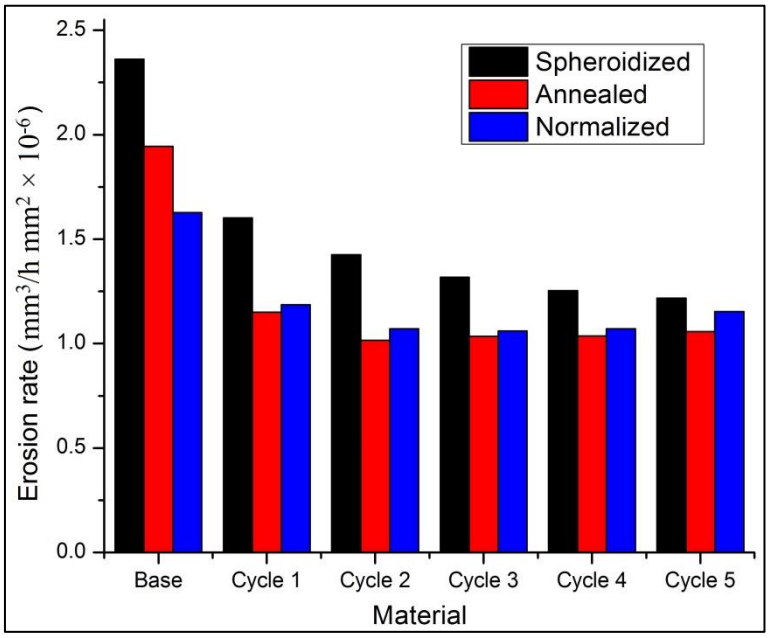

Fig. 5.16 Variation of average slurry erosion rate for different thermal cycled samples

Surface roughness of all polished samples before erosion test is 0.05µm. After slurry test, surface roughness increases due to cutting and ploughing of sand particles.

Variation of surface roughness values after 24 hour slurry test is shown in Fig. 5.17. This variation is well correlated with cumulative weight loss values and erosion rate values. Softer materials have high roughness than hard thermal cycled materials.

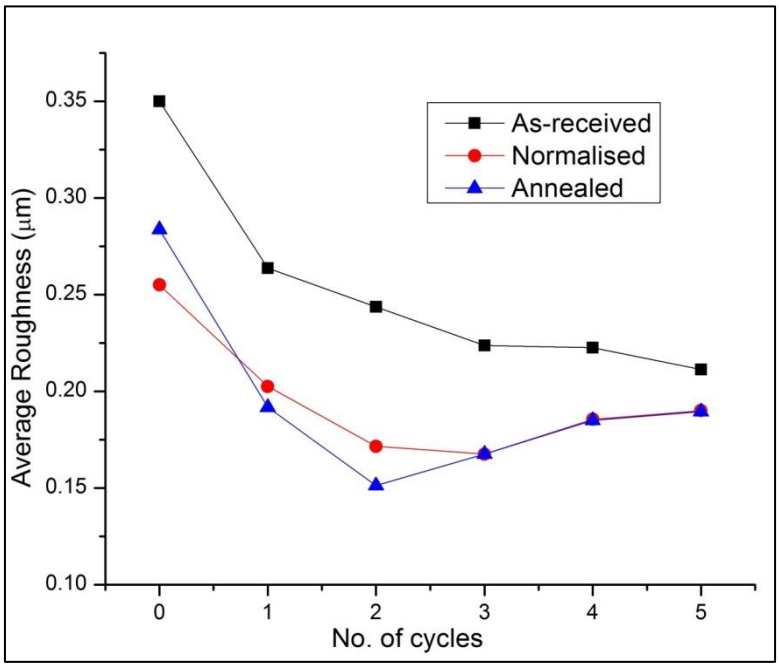

Fig. 5.17 Variation of average surface roughness for different thermal cycled samples

5.5 SEM analysis of eroded surfaces

Continuous impact of sand particles at different angles causes wear. Wear mechanism in case of slurry erosion mainly depends on material properties, slurry characteristics and angle of impact. Wear can be viewed as plastic deformation of ductile matrix, cutting of brittle phases, surface fatigue, abrasion erosion, lip, crater and pore formation. Cutting and plastic deformation are two main erosion mechanisms. At low impact angles, cutting dominates. At high impact angle, crater lip formation dominates. But in case of slurry erosion, water strikes at different impact angles over the surface and in present work, also, slurry erosion pot tester is designed such that sand particles strike the cylindrical samples at different angles.

To understand the erosion mechanism, worn out surfaces are examined under SEM. The circular surface which is normally impacted by the slurry flow is examined under SEM as it is most uneven or rough surface. However anyone cannot say that the

impact angle is 90º at this surface because impact angle for each sand particle is different depending on their morphology.

In case of spheroidized material, SEM micrograph shown in Fig. 5.18 clearly depicts the wear marks which are due to plastic deformation and cutting. The eroded surface of spheroidized base material is highly uneven. The mechanism of slurry erosion for spheroidized material is plastic deformation of ductile ferrite matrix and pull out of fine cementite particles. Continuous impact of sand particles plastically deforms the ferrite matrix and due to this, cementite particles partially come out of the surface. On further impact, cementite particles easily pull out of the surface. Pores seen in SEM micrograph reveal the pull out of cementite particles. Also it is clearly seen that on increasing thermal cycle, worn out surfaces are relatively smoother due to large cementite. Presence of cutting marks, pores, craters and lips can be seen on SEM images, which are accountable for weight loss.

The SEM images of worn out surface of annealed base and thermal cycled material are shown in Fig. 5.19. In this case, it is observed that craters and cutting is responsible for material removal. Crater lips formed due to impact of sand particles and lip break on further impact of erodent. Cutting action is observed mainly on thermal cycled samples, this may be due to worn out of brittle pearlite phase. The continuous impact of sand particles on brittle phases results in fatigue failure.

In case of ferrite-pearlite microstructure, ductile ferrite matrix is plastically deformed due to continuous impact of sand particles leaving brittle pearlite phase exposed. On further impingement of sand particles, cementite lamellae fractured. In case of annealed material, coarse pearlite is easily fractured because of large gap between ferrite and cementite phase.

The SEM images of worn out surface of normalized base and thermal cycled material are shown in Fig. 5.20. Wear marks are seen on the worn out surfaces which may be due to plastic deformation and cutting. Normalized base material is most uneven surface as large no. of craters are seen on eroded surface. These craters are responsible for weight loss. Material is also removed in form of crater lip fracture.

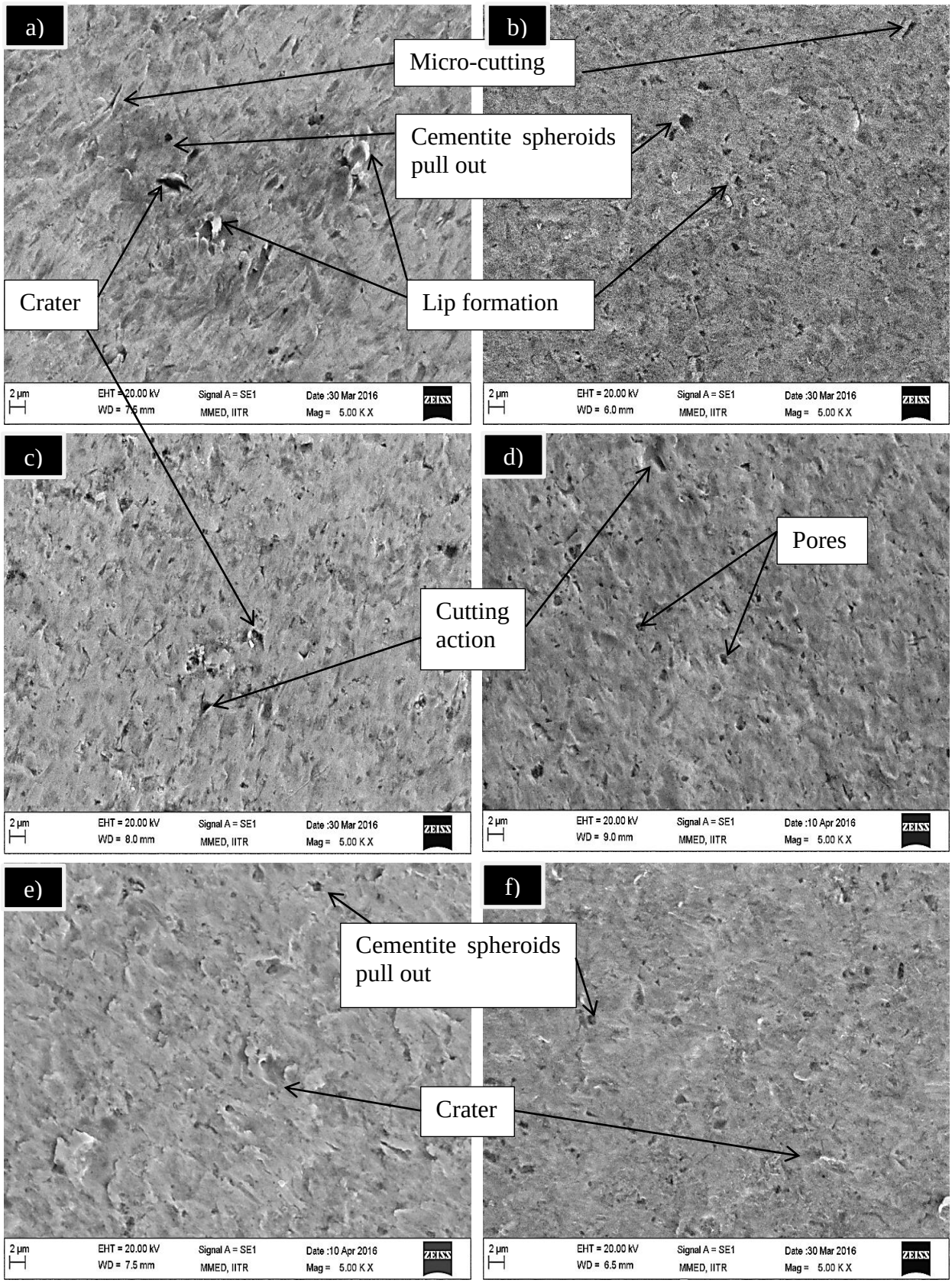

Fig. 5.18 SEM images of spheroidized base and thermal cycle samples after 24hr slurry erosion test: a) base; b) 1-cycle; c) 2-cycle; d) 3-cycle; e) 4-cycle; and f) 5-cycle

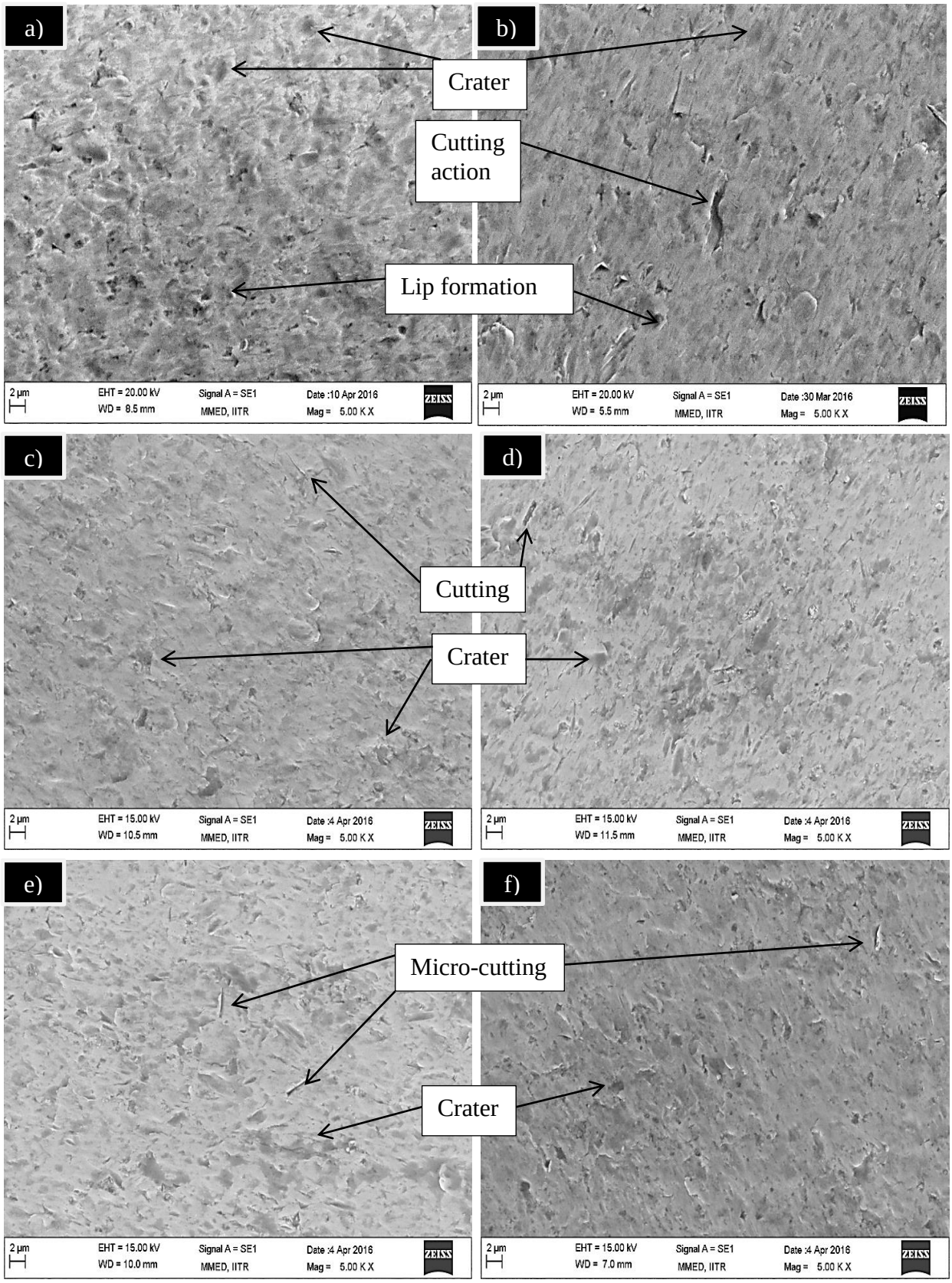

Fig. 5.19 SEM images of annealed base and thermal cycle samples after 24hr slurry erosion test: a) base; b) 1-cycle; c) 2-cycle; d) 3-cycle; e) 4-cycle; and f) 5-cycle

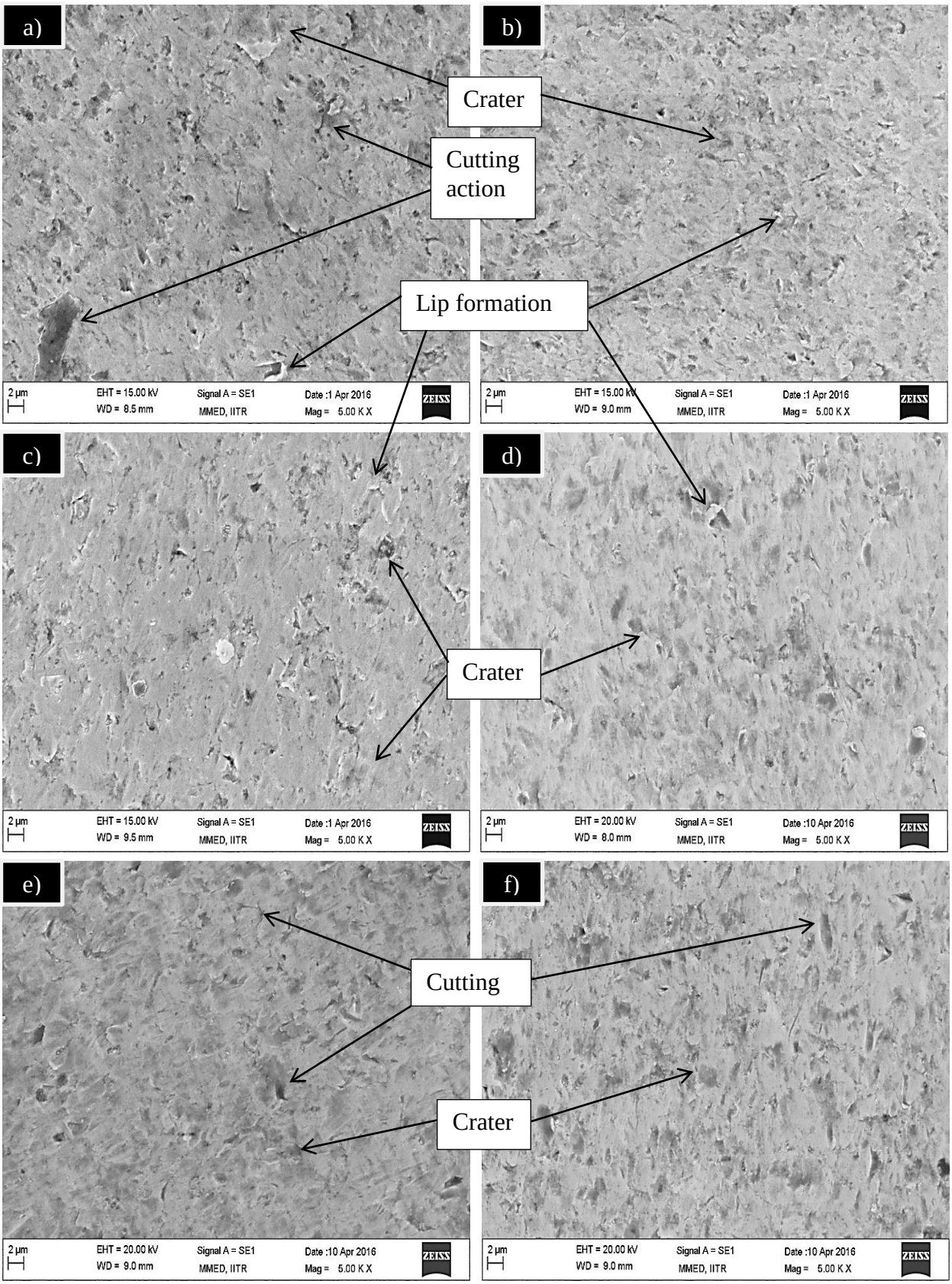

Fig. 5.20 SEM images of normalized base and thermal cycle samples after 24hr slurry erosion test: a) base; b) 1-cycle; c) 2-cycle; d) 3-cycle; e) 4-cycle; and f) 5-cycle

Chapter 6
Conclusion

1. Thermal cycling results in different microstructural characteristics for spheroidized, annealed and normalized materials. Cementite spheroid size increases with increase in thermal cycling and pearlite formation also observed after 4^{th} -5^{th} thermal cycle in case of spheroidized material. Grain refinement and fragmentation of cementite lamellae are two main morphological changes observed with increase in thermal cycling in case of annealed and normalized thermal cycling.
2. Thermal cycling effect on improving mechanical property is found maximum on annealed material due to its initial coarse grain structure.
3. Ultimate tensile strength and hardness increases due to grain refinement after thermal cycling but in case of annealed and normalized material, strength property decreases after 2^{nd} and 3^{rd} cycle respectively due to elimination of lamellar pearlite.
4. Slurry erosion resistance shows direct relationship with hardness. Minimum weight loss is observed in case of two time thermal cycled annealed material (57% decrement w.r.t. as-received spheroidized material).
5. Plastic deformation and cutting are two main mechanisms observed for material removal.

Chapter 7
Scope for future work

1. Thermal cycling in different regions may results in variety of microstructures and mechanical properties. There will be possibility to get better results by changing various parameters such as thermal cycling temperature zone, heating rate, cooling rate and holding time.
2. Descriptive slurry erosion testing at various parameters such as changing impingement angle, slurry concentration, erodent size, slurry velocity etc.
3. As slurry environment is also corrosion susceptive. So effect of thermal cycling on corrosion behaviour will be tested.

Chapter 8

References

[1] Z. Q. Lv, B. Wang, Z. H. Wang, S. H. Sun, and W. T. Fu : Effect of cyclic heat treatments on spheroidizing behavior of cementite in high carbon steel, Mater. Sci. Eng. A, 2013, vol. 574, pp. 143–148.

[2] A. Saha, D. K. Mondal, K. Biswas, and J. Maity : Development of high strength ductile hypereutectoid steel by cyclic heat treatment process, Mater. Sci. Eng. A, 2012, vol. 541, pp. 204–215.

[3] A. Saha, D. K. Mondal, K. Biswas, and J. Maity : Microstructural modifications and changes in mechanical properties during cyclic heat treatment of 0.16% carbon steel, Mater. Sci. Eng. A, 2012, vol. 534, pp. 465–475.

[4] R. Grange : Strengthening by austenite grain refinement, Transaction of American society of metals, 1966, vol. 59, pp. 26–29.

[5] Reza Abbaschian, Lara Abbaschian and Robert E. Reed-Hill : Physical Metallurgy Principles, 4th edition, Wadsworth Publishing Co., Washington, 2009, pp. 180–182.

[6] B. Smoljan : An analysis of combined cyclic heat treatment performance, J. Mater. Process. Technol., 2004, vol. 155–156, pp. 1704–1707.

[7] V. Singh, J. Vimal, and V. Chaturvedi : A study on development of industrial tribology in india with some future prospects, IJMIE, 2012, vol. 2231, pp. 2–5.

[8] A. Sharma, A. Kumar, and R. Tyagi : Erosive wear analysis of medium carbon dual phase steel under dry ambient condition, Wear, 2015, vol. 334–335, pp. 91–98.

[9] R. Chattopadhya : Surface Wear: Analysis, Treatment, and Prevention, ASM International, U.S.A., 2001, pp. 80–85.

[10] J. Y. Koo and G. Thomas : Thermal cycling treatments and microstructures for improved properties of Fe-0.12% C-0.5% Mn steels, Mater. Sci. Eng., 1976, vol. 24, pp. 187–198.

[11] A. Saha, D. K. Mondal, and J. Maity : Effect of cyclic heat treatment on microstructure and mechanical properties of 0.6 wt. % carbon steel, Mater. Sci. Eng. A, 2010, vol. 527, pp. 4001–4007.

[12] S. W. Mahajan, G. Venkataraman, and A. K. Mallik : Grain refinement of steel by cyclic rapid heating, Metallography, 1973, vol. 6, pp. 337–345.

[13] B. Karlsson : Grain refinement in Fe-C alloys by thermal cycling, Mater. Sci. Eng., 1973, vol. 11, pp. 185–193.

[14] T. Alam, M. Aminul Islam, and Z. N. Farhat : Slurry Erosion of Pipeline Steel: Effect of velocity and microstructure, J. Tribol., 2015, vol. 138, pp. 1–10.

[15] D. Kumar Goyal, H. Singh, H. Kumar, and V. Sahni : Slurry erosion behaviour of HVOF sprayed WC-10Co-4Cr and Al_2O_3+13TiO_2 coatings on a turbine steel, Wear, 2012, vol. 289, pp. 46–57.

[16] B. K. Gandhi and S. V. Borse : Effects of particle size and size distribution on estimating erosion wear of cast iron in sand-water slurries, Indian J. Eng. Mater. Sci., 2002, vol. 9, pp. 480–486.

[17] M. Lindgren and J. Perolainen : Slurry pot investigation of the influence of erodant characteristics on the erosion resistance of titanium, Wear, 2014, vol. 321, pp. 64–69.

[18] N. Ojala, K. Valtonen, A. Antikainen, A. Kemppainen, J. Minkkinen, O. Oja, and V.-T. Kuokkala : Wear performance of quenched wear resistant steels in abrasive slurry erosion, Wear, 2016, vol. 354, pp. 21–31.

[19] R. S. Lynn, K. K. Wong, and H. M. Clark : On the particle size effect in slurry erosion, Wear, 1991, vol. 149, pp. 55–71.

[20] Y. Iwai : Slurry wear properties of pump lining materials, Wear, 1997, vol. 210, pp. 211–219.

[21] M. A. Al-Bukhaiti, A. Abouel-Kasem, K. M. Emara, and S. M. Ahmed : Particle shape and size effects on slurry erosion of AISI 5117 steels, J. Tribol., 2016, vol. 138, pp. 1–8.

[22] R. Dasgupta, B. K. Prasad, A. K. Jha, O. P. Modi, S. Das, and A. H. Yegneswaran : Slurry erosive wear characteristics of a hard faced steel: effect of experimental parameters, Wear, 1997, vol. 213, pp. 41–46.

[23] A. H. Y. O.P. Modi, R. Dasgupta, B. K. Prasad, A. K. Jha, S. Das : Effect of sand concentration on slurry erosion of steels, Marerials Trans., 1998, vol. 39, pp. 1185–1190.

[24] M. A. Islam, T. Alam, Z. N. Farhat, A. Mohamed, and A. Alfantazi : Effect of microstructure on the erosion behavior of carbon steel, Wear, 2015, vol. 332–333, pp. 1080–1089.

[25] D. López, J. P. Congote, J. R. Cano, A. Toro, and A. P. Tschiptschin : Effect of particle velocity and impact angle on the corrosion-erosion of AISI 304 and AISI 420 stainless steels, Wear, 2005, vol. 259, pp. 118–124.

[26] A. V. Levy : Solid Particle Erosion and Erosion-corrosion of Materials, ASM International, Materials Park, OH, 1995, pp. 195–220.

[27] B. Yu, D. Y. Li, and A. Grondin : Effects of the dissolved oxygen and slurry velocity on erosion-corrosion of carbon steel in aqueous slurries with carbon dioxide and silica sand, Wear, 2013, vol. 302, pp. 1609–1614.

[28] M. A. Al-Bukhaiti, S. M. Ahmed, F. M. F. Badran, and K. M. Emara : Effect of impingement angle on slurry erosion behaviour and mechanisms of 1017 steel and high-chromium white cast iron, Wear, 2007, vol. 262, pp. 1187–1198.

[29] J. R. Laguna-Camacho, J. E. Escalante-Martinez, R. Cruz-Vicencio, J. V. Mendez-Mendez, I. Arzate-Vazquez, I. Hernandez-Romero, and M. Vite-Torres : Solid Particle Erosion Behaviour of TiN Coating on AISI 4140 Steel, J. Surf. Eng. Mater. Adv. Technol., 2014, vol. 4, pp. 1–8.

[30] G. T. Burstein and K. Sasaki : Effect of impact angle on the slurry erosion–corrosion of 304L stainless steel, Wear, 2000, vol. 240, pp. 80–94.

[31] N. Pereira Abbade and S. João Crnkovic : Sand-water slurry erosion of API 5L X65 pipe steel as quenched from intercritical temperature, Tribol. Int., 2000, vol. 33, pp. 811–816.

[32] N. Agarwal, G. P. Chaudhari, and S. K. Nath : Slurry and cavitation erosion of HSLA steel processed by warm multidirectional forging and inter-critical annealing, Tribol. Int., 2014, vol. 70, pp. 18–25.

[33] A. Kumar, A. Sharma, and S. K. Goel : Effect of heat treatment on microstructure, mechanical properties and erosion resistance of cast 23-8-N nitronic steel, Mater. Sci. Eng. A, 2015, vol. 637, pp. 56–62.

[34] B. Kishor, G. P. Chaudhari, and S. K. Nath : Slurry erosion of thermo-mechanically processed 13Cr4Ni stainless steel, Tribol. Int., 2016, vol. 93, pp. 50–57.

[35] R. Nafar Dehsorkhi, S. Sabooni, F. Karimzadeh, A. Rezaeian, and M. H. Enayati : The effect of grain size and martensitic transformation on the wear behavior of AISI 304L stainless steel, Mater. Des., 2014, vol. 64, pp. 56–62.

[36] S. G. Sapate, A. D. Chopde, P. M. Nimbalkar, and D. K. Chandrakar : Effect of microstructure on slurry abrasion response of En-31 steel, Mater. Des., 2008, vol. 29, pp. 613–621.

[37] V. Olden and Z. L. Zhang : Material characterisation for ductile fracture by testing of notched tensile specimens, Accepted for presentation on ECF14, Cracow, 2002, pp. 8-13.

[38] V. Olden, Z. L. Zhang, E. Ostby, B. Nyhus, and C. Thaulow : Notch tensile testing of high strength steel weldments, 2nd International Symposium on High Strength Steel, 2002, vol. 23-24, pp. 1–8.

[39] Z. L. Zhang, M. Hauge, C. Thaulow, and J. Odegard : A notched cross weld tensile testing method for determining true stress-strain curves for weldments, Eng. Fract. Mech., 2002, vol. 69, pp. 353–366.